FREQUENCY-SCALE EFFECT IN ELASTIC PERIODIC MULTI-LAYERED MEDIA

A Thesis

Presented to

the Faculty of the Department of Geosciences

University of Houston

In Partial Fulfillment

of the Requirements for the Degree

Master of Science

By

Juan Paulo Perdomo

December 2012

FREQUENCY-SCALE EFFECT IN ELASTIC PERIODIC MULTI-LAYERED MEDIA

Juan Paulo Perdomo

APPROVED:

Dr. John Castagna

Dr. Evgeni Chesnokov, Co-Chairman

Dr. Alfonso Gonzales

Dean, College of Natural Sciences and Mathematics

Acknowledgements

I have been blessed with friends and professors during the process of making this thesis. I would like to thank all of those who in one way or the other have helped me not only with my professional development but also in my personal growth. People like Constantin Lupascu, Jose Olaya and his family, Antonio Olaiz, Miguel Angel, and my Padre have taught me and given me the strength to continue with my studies and with many other projects in my life.

I would like to express my foremost gratitude to Dr. Castagna and Dr. Chesnokov for their continuous support, advice, and help during my studies at the University of Houston.

I am also indebted to Cintia Lapilli and Carlos Cobos for their comments, ideas, suggestions, clearcut answers, and discussions about this work and many other subjects that contributed to my understanding of the physics involved in wave propagation, rock physics and geophysics in general.

to my parents
Mercedez Tellez de Morales
and Miguel A. Morales

LavsDeo

FREQUENCY-SCALE EFFECTS IN ELASTIC PERIODIC MULTI-LAYERED MEDIA

An Abstract of a Thesis

Presented to

the Faculty of the Department of Geosciences

University of Houston

In Partial Fulfillment

of the Requirements for the Degree

Master of Science

By

Juan Paulo Perdomo

December 2012

Abstract

In general, a reservoir is formed by laminated layers of shale, sand, and other types of lithologies. Each layer has different elastic properties that are described by its own stiffness tensor (C_{ijkl}), density(ρ_j), and thickness (d_j), j being the number of the layer. A periodic medium is defined as the stack of homogeneous layers with different elastic properties that it repeats after some length (d), where d is called the period of the medium. If a wave-field travels through this periodic medium composed of isotropic layers, the wave shows two mutually exclusive behaviors. When the wavelength (λ) is smaller than d, the wave behaves as if in an isotropic medium but when λ is bigger than d, the wave behaves as if in an equivalent transversely anisotropic medium (Postma,1955; Rytov,1956; Rich,2006).

The goals of this thesis are three-fold. The first one is to describe the physical behavior of wave velocity as a function of thickness d and the impedance contrast between constituents when P-, S_v-, and S_h-wave travels in a periodic medium. The second goal is to quantify, in term of thickness of the period of the medium, the frequency and wavelength values at which the medium behaves as an effective anisotropic one. The third goal is to compute the seismic response of this elastic

periodic medium.

The description of how the wavefield propagates through the medium is given by the solution of the wave equation for elastic media. This solution allows the definition of Brillouin zones whose width is equal to π/d and shows that the periodic medium exhibits a range of stop-bands frequencies where the wave does not propagate. These stop-bands are located at the boundary of the Brillouin zone for the all of the types of waves (P, S_v, and S_h). In the case of P and S_v-waves, there are also stop-bands inside the Brillouin zone that depend on the frequency and angle of incidence of the wavefield. As a result, seismic response and dispersion relationships show that the medium can be considered anisotropic when $\lambda > 10d$ and this anisotropic behavior is also a function of the wavefield frequency (ω), for instance if the medium has a period of $d = 30m$, the medium is anisotropic for $\omega \leq$10hz.

Table of Contents

List of Figures

Introduction

Sedimentary basins are composed of stacks of layers with a wide range of variable thickness. A periodic medium is defines as the stack of homogeneous layers with different elastic properties that repeats after some length d; this d is the period of the medium. In nature these periodical structures are found at small and large scales. On small scale, the laminar characteristics of shales has been modeled as periodic medium (Vernik and Nur, 1996). On large scale, alternating layers of limestones and shales have been found and they can be considered as periodic media (Coe *et al.*, 2003).

In seismology, each of the medium layer is described by its elastic properties: the stiffness tensor (C_{ijkl}), density (ρ_j), and thickness (d_j), where j is the index of each layer. When an elastic wave field travels through a medium, it produces three displacement components associated with three type of waves. The S_h- and S_v-waves are waves with displacement perpendicular to the direction of the wave propagation and the P-wave has displacement parallel to the direction of propagation. This thesis studies the physical behavior when an elastic wave travels in a periodic medium. The thesis is divided into three chapters. In the first chapter, the theoretical background

for the solution of the wave equation in a periodical isotropic medium is presented. In chapter two, the solution for the wave equation for the S_h-wave and its dispersion relationship is derived. In chapter three, the solution for the wave equation for the P- and S_v-wave and their dispersion relationships are computed.

Dispersion relationships for all three waves show the existence of stop-bands at the boundary of the Brillouin zone and a modulation behavior. In this study, it is shown that the width of these stop-bands and their modulation is a function of wave incidence angle, thickness, and impedance contrast between constituents of the medium. Seismic response is computed using dispersion relationships and Green's function.

Wave propagation in a periodic laminated media has been the object of study of many authors. Postma (1955) and Rytov (1956) studied this type of media and computed the effective stiffness tensor for a wave propagating perpendicular, parallel and at angle of 45° from the vertical axis. Sun *et al.* (1968) and Sve (1971) computed the P- and S_v-wave dispersion relationship for waves traveling perpendicular, parallel and at different angles from the direction of bedding of the medium. Helbig (1984) studied the behavior of the S_h-wave when it travels through a periodic medium and found the S_h-dispersion relationship for the first Brillouin zone. Rich (2006) in his study, showed that the dispersion relationship of S_h-wave traveling at any angle also has stop-bands; this stop-band width is a function of impedance contrast between constituent of the medium. He also showed the existence of critical angle at which the S_h-wave dispersion relationship does not have any stop-bands. This thesis

complements Rich's findings in the following aspects: the modulation character of the dispersion relationship as function of the period thickness and impedance contrast is shown, the dependence of the stop-band width as a function of the constituents thickness is computing, stop-bands within the Brillouin zone for the P- and S_v-wave dispersion relationship are shown, the critical angle of the S_h-wave as a function of the impedance contrast of constituents is calculated, and a medium anisotropic factor is computed as a function of the frequency for different medium periods.

Chapter 1

Elastic wave equation in a periodic layered medium

1.1 Introduction

In this section the elastic wave equation for a periodic isotropic medium is defined in terms of different wave type: P-, S_v-, and S_h-waves. The medium is assumed infinite and composed of two constituents with different lithologies. In order to find a solution for the wave traveling in this medium, the Floquet Theorem is assumed, and the Helmholtz's Theorem is used to separate the displacement produced by the wavefield into three components that correspond to the P-, S_v-, and S_h-waves, respectively.

1.2 Wave equation in periodic layered medium

The wave equation for a infinite medium composed of alternating layers of two homogeneous and isotropic lithologies (periodic layered medium) is given by (Postma,1955; Rytov,1956; Sve,1971; Rich,2006):

$$\rho\left(x_3\right)\frac{\partial^2 u_i}{\partial t^2}=\frac{\partial}{\partial x_j}\left(C_{ijkl}\left(x_3\right)\frac{\partial u_k}{\partial x_l}\right) \tag{1.1}$$

In this equation the Einstein sum convection over repeated index is followed and index i represents each component. The geometry of the medium is shown in Figure 1.1, where it can be seen that the density and stiffness tensor depend only on the coordinate x_3 for the whole medium, but each constituent is considered homogeneous and isotropic.

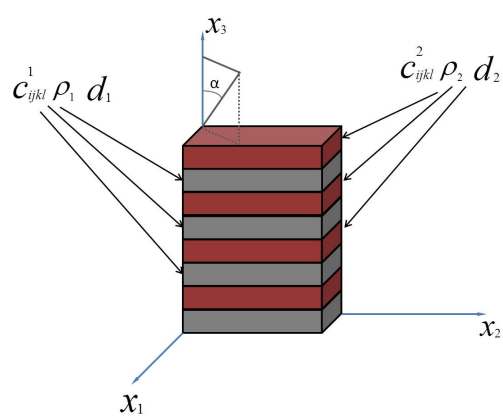

Figure 1.1: Periodical laminated medium

The Floquet Theorem or Block Theorem has been applied to the analysis of the propagation of waves through composite media with periodic structure (Rytov,1956;

Lee at al.,1973; Sve,1971; Rich,2006). According to the Floquet Theorem, if $F(x)$ is the solution to the wave equation of the periodic medium then F(z) is a periodic function with period d of the medium such that $F(x) = F(x+d)$. Using this theorem, the solution of the wave equation will be the solution of the wave equation for the two constituents considering separately, and then solution is constrained to be a periodic function with the period of the medium $d = d_1 + d_2$ (Rytov,1956; Sve,1971; Rich,2006). The physical effect of the Floquet Theorem is to compute the wave equation for the two constituents and then weld the two ends of this medium with the same array of constituents in order to build the infinite periodical medium. This assumption is valid since all the physical property of the medium: stiffness tensor, density, and thickness are periodic function of the x_3 coordinate with the period d. The effect of applying the Floquet Theorem to equation 1.1 is:

$$\rho^p \frac{\partial^2 u_i^p}{\partial t^2} = C_{ijkl}^p \frac{\partial}{\partial x_j} \left(\frac{\partial u_k^p}{\partial x_l} \right) \tag{1.2}$$

where index p represents the layer number.

In order to solve this equation for this periodical medium, I follow the procedure outline by Rytov (1956) and Rich (2006). A plane wave that propagates in the direction x_2x_3 plane is assumed, this is valid since the medium has a vertical symmetry. I also use Helmholtz's Theorem to separate the displacement into vector potential

($\boldsymbol{\psi}$) and scalar potential (ϕ) in the form (Aki:1980; Rich,2006):

$$\boldsymbol{u} = \nabla\phi + \nabla \mathrm{x} \boldsymbol{\psi} \tag{1.3}$$

Where bold letters denotes vectors and ∇ denotes the vector differential operator.

Replacing equation 1.3 in 1.1 and knowing that $C_{ijkl} = \lambda\delta_{ij}\delta_{kl} + \mu\left(\delta_{ik}\delta_{jl} + \delta_{il}\delta_{jk}\right)$ for isotropic layers, I have the following equations

$$\begin{aligned}
\rho\frac{\partial^2\phi}{\partial t^2} &= (\lambda + 2\mu)\left(\frac{\partial^2\phi}{\partial x_1^2} + \frac{\partial^2\phi}{\partial x_2^2} + \frac{\partial^2\phi}{\partial x_3^2}\right), \\
\rho\frac{\partial^2\psi_1^*}{\partial t^2} &= \mu\frac{\partial^2\psi_1^*}{\partial x_1^2}, \\
\rho\frac{\partial^2\psi_2^*}{\partial t^2} &= \mu\frac{\partial^2\psi_2^*}{\partial x_2^2}, \\
\rho\frac{\partial^2\psi_3^*}{\partial t^2} &= \mu\frac{\partial^2\psi_3^*}{\partial x_3^2}
\end{aligned} \tag{1.4}$$

where $\psi_i^* = \psi_{j,l} - \psi_{j,l}$ is the ith-component of the curl and the symbol ”,” denoted coordinate derivative. Equation 1.4 allows separation of the problem in to two cases. In the first case, the displacement field is in the plane x_3x_2. In the second case, the propagation is perpendicular to the plane x_3x_2. The first case corresponds to P and S_v waves while the second corresponds to S_h waves.

This document uses the procedure to solve the equations 1.4 given by Rich (2006) with some clarifications.

Chapter 2

$\mathbf{S_h}$-wave equation solution

2.1 Introduction

In previous chapter it was showed how the Floquet's Theorem was used to simplify the wave equation and how the Helmhotz's Theorem allowed the separtion of the wavefield into P- S_v- and S_h-waves. In this chapter a solution of the S_h-wave and its dispersion relationship is found using the methodology presented in Rich (2006). This relationship is analyzed as a function of the wave incidence angle, the medium period thickness(d) and the S-impedance contrast of the medium.

2.2 $\mathbf{S_h}$ wave solution

the S_h-wave is assumed to be perpendicular to the y-z plane. Since Helmholtz's Theorem is assumed, the vector-potential ψ in the x-direction is the only one that describes the displacement in the x-direction. This means that $u_z = 0$, $u_y = 0$ and

$u_x = \psi_{y,x} - \psi_{z,y} = \psi_x^*$, the wave equation in this case is:

$$\rho \frac{\partial^2 \psi_x^*}{\partial t^2} = \mu \left(\frac{\partial^2 \psi_x^*}{\partial y^2} + \frac{\partial^2 \psi_x^*}{\partial z^2} \right) \tag{2.1}$$

A solution in the form of plane waves times a function that depends on the variable z, ψ_x^* is equal to

$$\psi_x^* = g_j(z) e^{i(k_z z + k_y y - wt)} \tag{2.2}$$

Substituting equation 2.2 for ψ_x^* into 2.1, the function $g(z)$ has to obey below differential equation:

$$\frac{\partial^2 g_j}{\partial z^2} + 2ik_z \frac{\partial g_j}{\partial z} + \left(\frac{w^2}{c_{tj}^2} - k_z^2 - k_y^2 \right) g_j = 0 \tag{2.3}$$

The subscript j is the layer number, $\beta_j = \sqrt{\frac{w^2}{V_{sj}^2} - k_y^2}$ and V_{sj} is the V_s-velocity of the jth-layer. Hence, the solution to 2.3 has the form:

$$g_j(z) = E_j e^{-iz(k_z + \beta_j)} + F_j e^{-iz(k_z - \beta_j)} \tag{2.4}$$

and the solution to the displacement u_x is

$$u_x = \sum_{j=1}^{2} \left[E_j e^{-iz\beta_j} + F_j e^{iz\beta_j} \right] e^{i(k_y y - wt)} \tag{2.5}$$

The value of the constants F_j and E_j can be obtained by applying the continuity of displacement and stress at the boundary $z = 0$, $z = -d_2$ and $z = d_1$. These

boundary conditions are:

$$
\begin{aligned}
u_x\left(0^-\right) =& u_x\left(0^+\right), & \sigma_{xz}\left(0^-\right) =& \sigma_{xz}\left(0^+\right), \\
u_x\left(d_1\right) =& u_z\left(-d_2\right) e^{(ik_z d)}, & \sigma_{xz}\left(d_1\right) =& \sigma_{xz}\left(-d_2\right) e^{(ik_z d)}, \\
& & d =& d_1 + d_2
\end{aligned}
\tag{2.6}
$$

The last three equations impose the periodicity of the wave-field required by the Floquet Theorem. Using $u_x = \psi^*$ and $\sigma_{xz} = \mu u_{x,z}$, the matrix equation for the coefficient E_j and F_j is:

$$
\begin{pmatrix}
1 & 1 & -1 & -1 \\
-\beta_1\mu_1 & \beta_1\mu_1 & \beta_2\mu_2 & -\beta_2\mu_2 \\
e^{-id_1(k_z+\beta_1)} & e^{-id_1(k_z-\beta_1)} & -e^{id_2(k_z+\beta_2)} & -e^{id_2(k_z-\beta_2)} \\
-\beta_1\mu_1 e^{-id_1(k_z+\beta_1)} & \beta_1\mu_1 e^{-id_1(k_z-\beta_1)} & \beta_2\mu_2 e^{id_2(k_z+\beta_2)} & -\beta_2\mu_2 e^{id_2(k_z-\beta_2)}
\end{pmatrix}
*
\begin{pmatrix} E_1 \\ F_1 \\ E_2 \\ F_2 \end{pmatrix} = 0
\tag{2.7}
$$

The solution in 2.7 is found when the determinant of the matrix is equal to zero. Appendix one shows the mathematical process to solve the determinat of equation 2.7 and to derive the equation that relates k_z to the physical properties of the medium (ρ_j, thickness and V_{sj}). This expression was also derived by Helbig (1984) using a different method. This equation is:

$$
cos(k_z d) = cos(\beta_1 d_1)cos(\beta_2 d_2) - \frac{(m_1/m_2 + m_2/m_1)}{2} sin(\beta_1 d_1)sin(\beta_2 d_2) \tag{2.8}
$$

where

$$\beta_j = \sqrt{\left(\frac{\omega}{V_{sj}}\right)^2 - k_y^2}$$

$$m_j = \mu_j \beta_j = \sqrt{\mu_j \rho_j}\omega \frac{\sqrt{\left(\frac{\omega}{V_{sj}}\right)^2 - k_y^2}}{k_j}$$

j is the number of the layer in the medium and V_{sj} is the V_s-velocity of the jth-layer.

Equation 2.8 is solved for the values of k_z. This solution gives the dispersion relationship that relates the wave number k_z and as a function of the frequency w and k_y. Equation 2.8 has the same general form as the one obtained by Helbig (1984) and Rich (2006), however the variable m_j is different from the one reported by Rich (2006) by a factor ω. This difference does not alter the final result from equation 2.8, since in this equation the ratio between m_1 and m_2 (m_1/m_2 and m_2/m_1) cancels out this ω factor. In the rest of this chapter, analysis of this relationship is done in terms of impedance contrast and thickness of the constituents.

2.3 Dispersion of S_h-waves traveling perpendicular to layering

The first case to be analyzed for the dispersion equation 2.8 is when the S_h-wave is traveling perpendicular to the layers. This means that $\beta_j = \rho_j \frac{w}{\mu_j}$ and equation 2.8 takes the form:

$$cos(k_z d) = cos(\frac{\omega}{v_1} d_1) cos(\frac{\omega}{v_2} d_2) - \frac{1+\chi^2}{2\chi} sin(\frac{\omega}{v_1} d_1) sin(\frac{\omega}{v_2} d_2) \tag{2.9}$$

where $\chi = \frac{v_2\rho_2}{v_1\rho_1}$. This equation was first obtained by Rytov (1956) and gives explicit values for k_z when it is solved for a given ω. An example of this solution is given in Figure 2.1 using the values of velocity and density for the two constituents given in Table 2.1. This table is taken from Rich (2006) but with different constituent thicknesses, he used $1m$ thickness for both constituents. The reason of this change in thickness is to always make a comparison of how the constituent thicknesses affects the dispersion relationship. The result of this solution is the spectrum of the S_h-wave traveling perpendicular to the layer ($\alpha = 0$).

	Sand	Shale
$V_p\,[km/s]$	4.00	2.00
$V_s\,[km/s]$	2.36	0.67
$\rho\,[gr/cm^3]$	2.37	2.10
$\lambda\,[Gpa]$	11.52	6.50
$K\,[Gpa]$	2.37	2.10
$\mu\,[Gpa]$	13.14	0.94
$d_j\,[m]$	10.0	20.0

Table 2.1: Properties for sand-shale periodic medium, taken from Rich (2006).

The solution of equation 2.9 is shown in Figure 2.1. This solution has two important features: the first is that the solution is periodical with the period equal to $2\pi/d$ and the second is that there are some frequencies at which there are no k_z values, these ranges of ω with no k_z are called stop-bands (Brillouin, 1946). Brillouin demonstrated that the physical wave behavior in a periodic media can be fully described only if wavenumber, k_z, is considered within the range:

$$-\frac{\pi}{d} \leq k_z \leq \frac{\pi}{d} \tag{2.10}$$

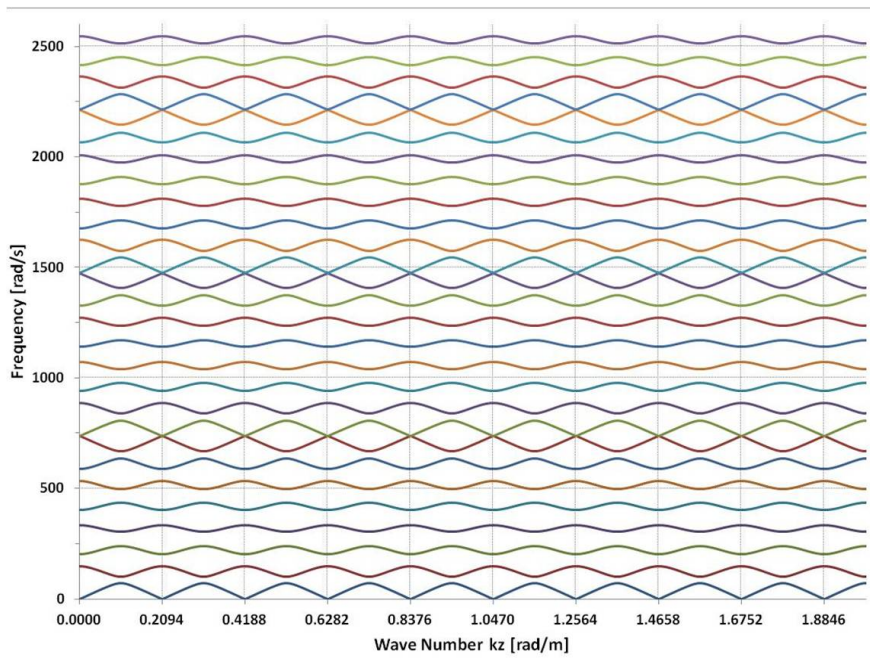

Figure 2.1: Spectrum of V_{sh}-wave, wavenumber k_z as a function of frequency(ω) for d=30m.

The zone where this k_z has these values is called "Brillouin zone" in his honor, borrowing this concept from his work in solid state physics. This periodicity in the dispersion function is a direct consequence of Floquet Theorem since the solution of the wave equation is constrained to be periodic. The stop-bands occur at the boundary of the Brillouin zones, where multiple reflections are in phase which add constructively and produce scattering that does not allow the wave to propagate at such frequencies (Marion *et al.*, 1994).

Since the solution to equation 2.9 is periodic and also an even function of k_z, this means that $\omega(k_z) = \omega(-k_z)$. This characteristic allows representation of the dispersion relationship using two different diagrams: the reduced diagram and the extended one (Lee and Yang, 1973). These two diagrams are shown in Figure 2.2.

The reduced diagram considers only those wavenumbers between zero and half the period ($0 \leq k \leq \frac{\pi}{d}$) of the dispersion relationship.

On the other hand, the extended diagram considers the positive range of k_z of the dispersion relationship. This extended representation can be obtained by two equivalent ways. The first method is to use the reduced diagram and unfold the values of $\omega(k_z)$ with respect to the axis $k_z = \pi/d$ as shown in Figure 2.2. The number on the side in each curve in this figure shows how the curves have been unfolded.

The other method uses the complete solution of equation 2.9 for the whole positive range of k_z as it is shown in Figure 2.1, and selecting the values of $\omega(k_z)$ that correspond to different curves in each Brillouin zone. Figure 2.3 shows the dispersion curves of Figure 2.1 plotted in this manner.

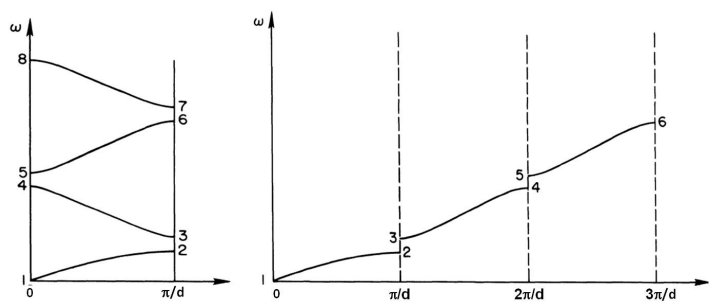

Figure 2.2: Example of the reduced representation (left) and extended representation (right). The number in the curves show the relationship between these two representations, from Lee and Yang (1973) .

The extended scheme facilitates evaluation of the phase velocity for the S_h-wave since the phase velocity is equal to $w(k_z)/k_z$. This is shown in Figure 2.3. In this graph, the presence of stop-bands is also evident as it was described before.

The length of these gaps depends on the S-impedance contrast between the two constituents and their corresponding thickness. In the next section a detailed study of this feature is done.

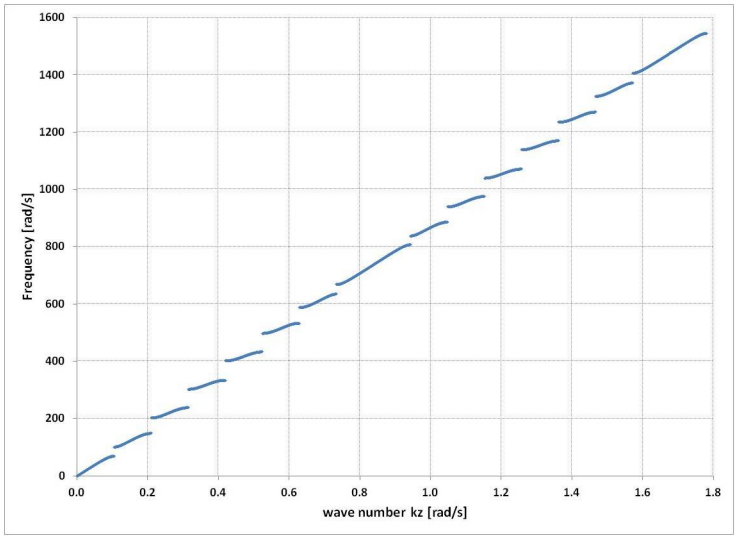

Figure 2.3: Extended zone scheme for S_h-wave with a periodic medium with the physical properties shown in Table 2.1

2.3.1 $\mathbf{S_h}$-wave phase velocity as a function of frequency

One of the important results of the dispersion function is that it allows computation of the phase velocity as a function of the frequency, which is shown in Figure 2.4. This figure shows two features: the phase velocity as a modulated function of the frequency and that at large frequencies ($\omega \geq 2000$ rad/s), phase velocities converge to a velocity value of 880.1 m/s (red dash line in figure). This velocity corresponds to the velocity computed using the ray theory. This theory will be explained in a later section.

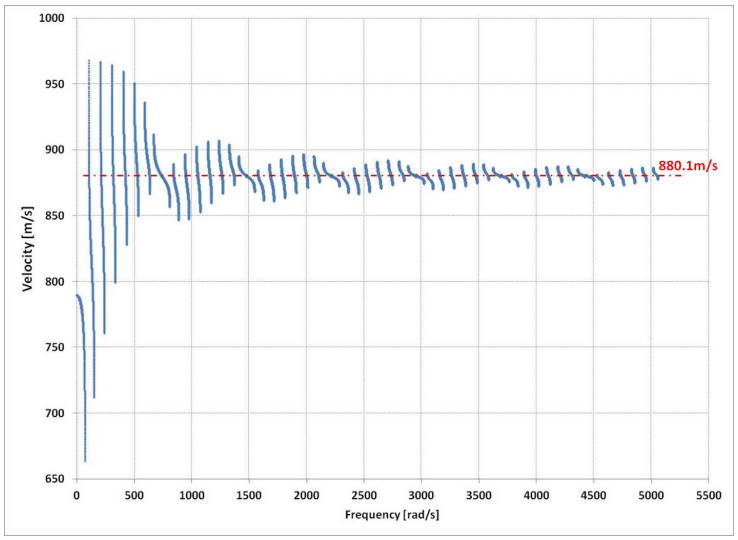

Figure 2.4: Phase velocity as a function of frequency ω for a periodic medium with the physical properties shown in Table 2.1. Red dashed line shows the Ray Theory velocity at 880.1 m/s

The two physical factors that influence the modulation of the phase velocity as a function of the frequency (ω) are the thickness and the velocity contrast of the constituents. As an example of this, Figure 2.5 and Figure 2.6 show how the modulation changes when each of these factors is changed and the other is kept constant. Figure 2.5 shows that the modulation is higher when the thickness of the medium that has the slowest velocity is thicker than those with a faster velocity. In this figure, it is also shown that the phase velocity converges to the Ray Theory velocity and that this Ray Theory velocity changes as the thickness of the constituents change.

Figure 2.6 shows the change in the modulation when the V_s-contrast between constituents changes. The result is that the modulation character is more evident when the contrast between the Vs of the constituents is small ($\leq 40\%$).

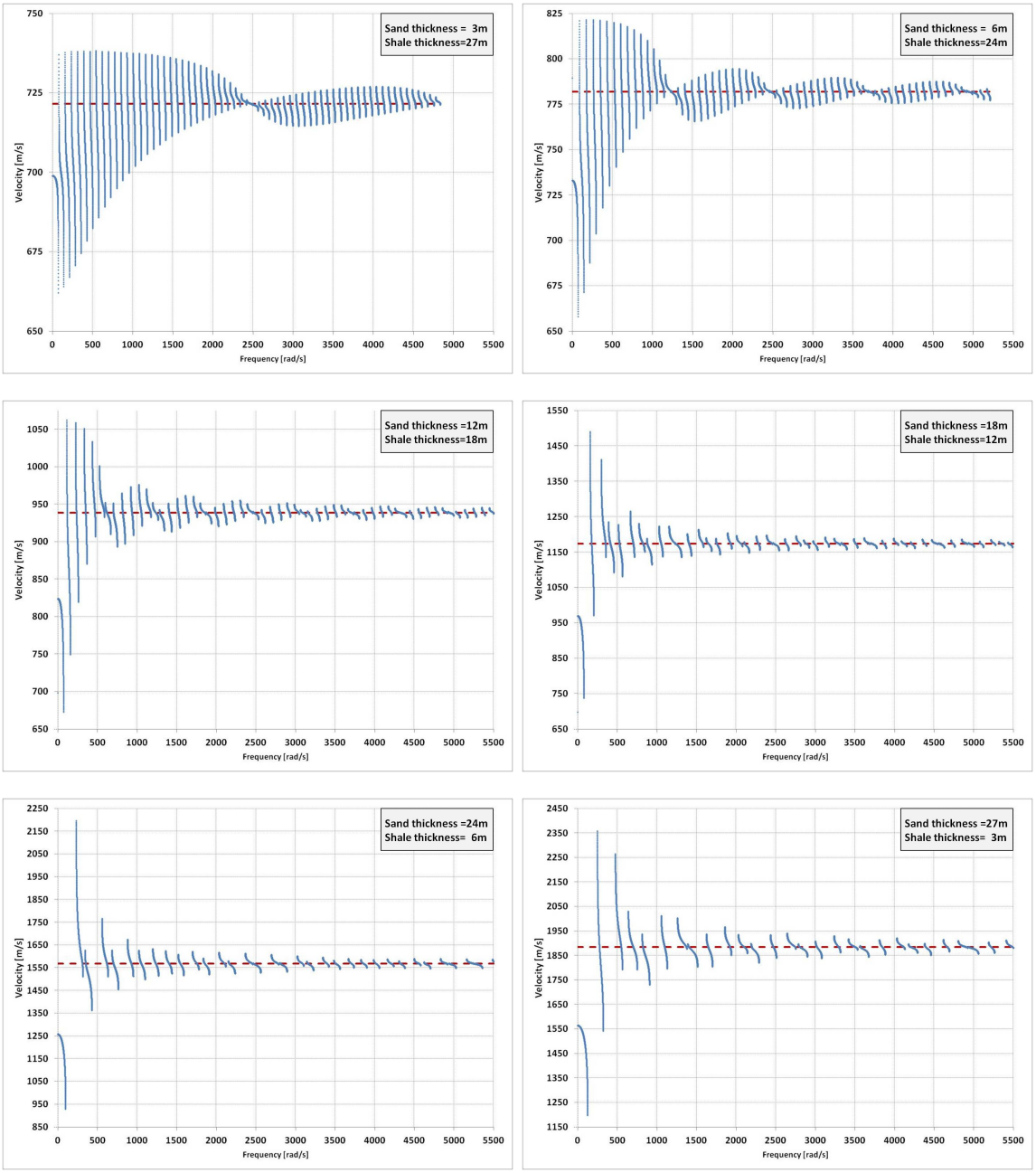

Figure 2.5: Phase velocity as a function of frequency ω for a periodic medium, the velocity and density are kept as in Table 2.1 but the constituent thicknesses change as is shown in top of each panel. Red dashed line shows the Ray Theory velocity.

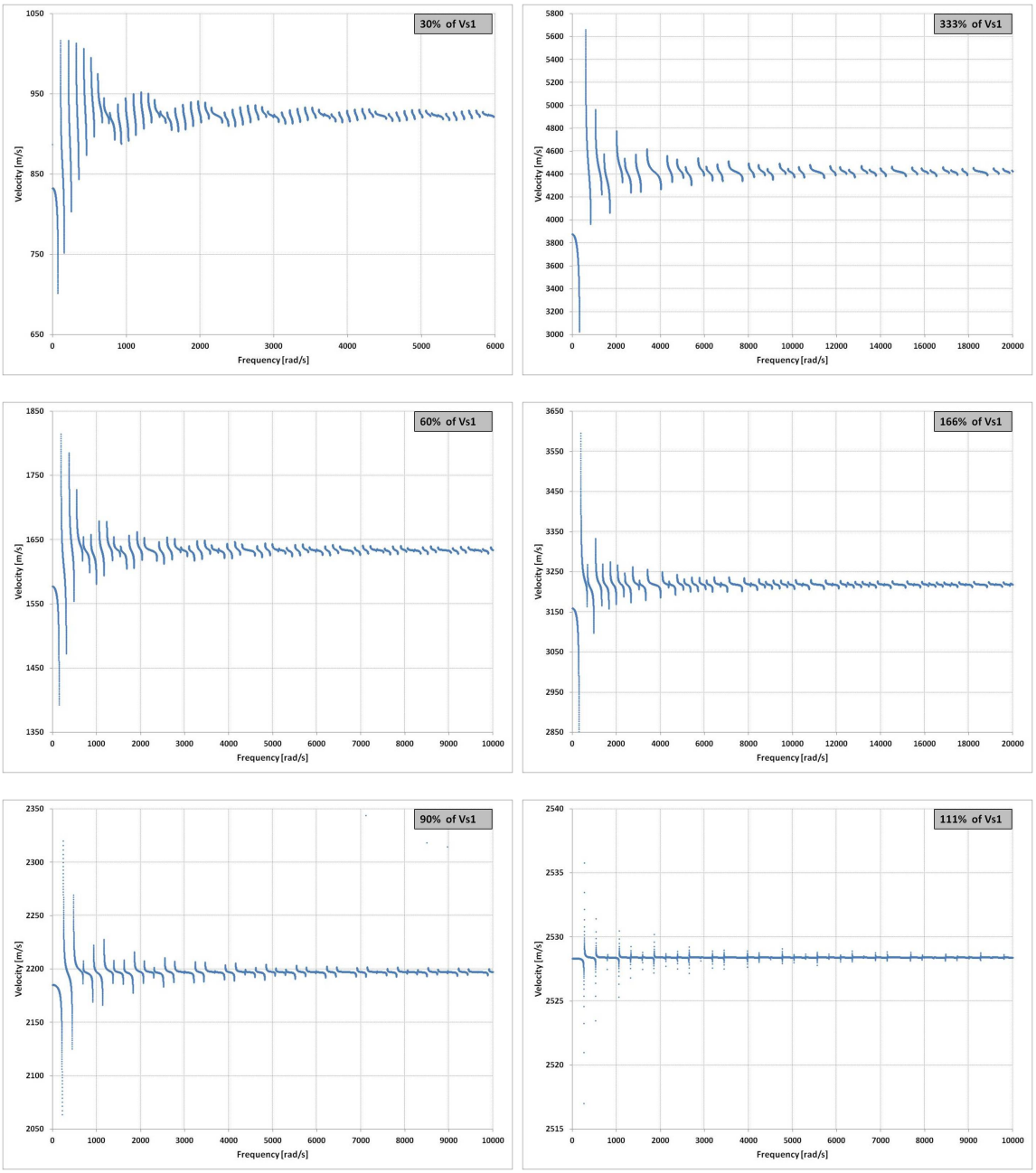

Figure 2.6: Phase velocity as a function of frequency ω for a periodic medium, the thickness and density are kept constant as in Table 2.1 but the V_s-shale velocity changes as a percentage of the V_s-sand velocity, the percentage values are shown in top of each panel.

2.3.2 S_h-wave phase velocity as a function of wavelength

Figure 2.7 shows the phase velocity as a function of the ratio between the wavelength and the thickness of the period of the medium ($\frac{\lambda}{d}$). This figure shows that the V_{sh} phase velocity can be approximated similar to the velocity computed through the Effective Media Theory (green line in Figure 2.7) at large wavelengths compared with d. On the other hand, if the wavelength is much smaller than d, the phase velocity can be approximated as the velocity computed by the Ray Theory (red line in Figure 2.7). These two theories explain how the medium behaves in the limit cases. When the wavelength is comparable with d ($\lambda \approx d$), a lot of dispersion effects take place, mainly due to scattering phenomena (Marion *et al.*, 1994). This is observed in Figure 2.7 when $0.1 > \frac{\lambda}{d} < 10$.

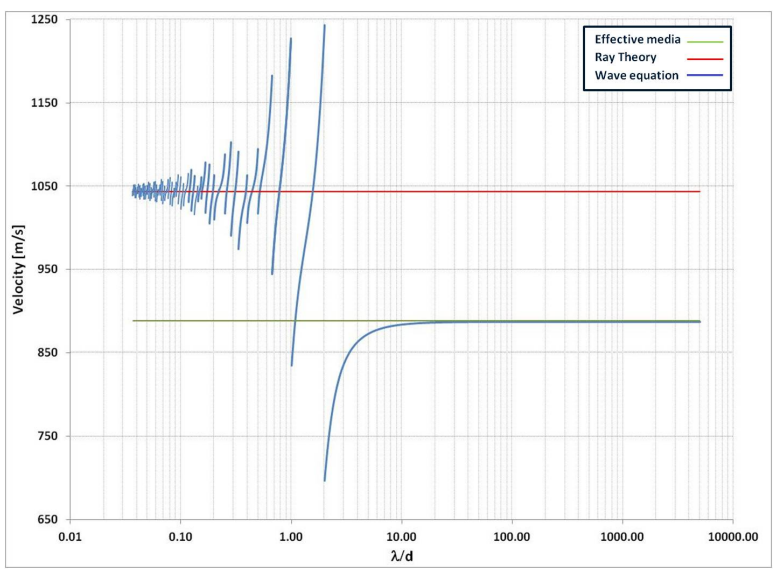

Figure 2.7: Phase velocity as a function of the thickness ratio λ and the period thickness d for a periodic medium with the physical properties shown in Table 2.1. The lines in green and red show the velocity using Ray and Effective Media Theory respectively.

2.3.3 Ray and Effective Medium Theory

Before continuing with the description of the wave traveling in a periodic media, a few comments about the Ray and Effective Medium Theory are needed. The Ray Theory occurs when wavelength is much less than the layer thickness ($\lambda \ll d$). It assumes that all constituents experience the same strain, and this is represented by the isostrain or Voigt bound (Mavko *et al.*, 2003). In this case the total elastic modulus of the whole media is computed using the equation:

$$M_{ray} = \sum_{j=1}^{2} f_j M_j \tag{2.11}$$

where the M_j is the elastic modulus of the jth-layer, and f_j is the fraction of volume the jth-layer. In order to compute the phase velocity of the whole media, the time average, also known as Wyllie's Equation is used (Wyllie *et al.*, 1956)

$$V_{ray}^{-1} = \sum_{j=1}^{2} \frac{f_i}{V_j} \tag{2.12}$$

On the other hand, The Effective Medium Theory occurs when the wavelength is much greater than the layer thickness ($\lambda \gg d$). In this theory, it is assumed that all the constituents experience the same stress, representing the isostress or Reuss bound (Mavko *et al.*, 2003). In this case the total elastic modulus of the whole media

is computed using the equation:

$$M_{ray} = \left(\sum_{j=1}^{2} f_j M_j \right)^{-1} \tag{2.13}$$

where the M_j is the elastic modulus of the jth-layer, and f_j is the fraction of volume of the jth-layer. In order to compute the effective phase velocity of the whole media, the below equation is used:

$$\begin{aligned} V_{eff}^{-1} =& \rho_{aver} \sum_{j=1}^{2} \frac{f_i}{\mu_j} \\ \rho_{aver} =& \sum_{j=1}^{2} f_i \rho_j \end{aligned} \tag{2.14}$$

These two theories explain how the medium behaves in the limit cases: $\lambda \gg d$ and $\lambda \ll d$

2.3.4 Dependence of the gap width with S-impedance contrast and layer thickness

The dispersion relationship for a wave propagating in periodic media shows the presence of stop-bands or gaps. These gaps, localized at the boundary of the Brillouin zone, are defined as frequency bands at which the wave can not propagate. The phenomenon is explained as the presence of multiple reflections that are in phase at the Brillouin boundary attenuating the wave at these boundaries (Marion *et al.*, 1994). In this section the width of this gap is analyzed as a function of the of the impedance contrast and thickness changes of the constituents. Figure 2.8 shows an

example of how these gaps change when the thickness of the constituents changes.

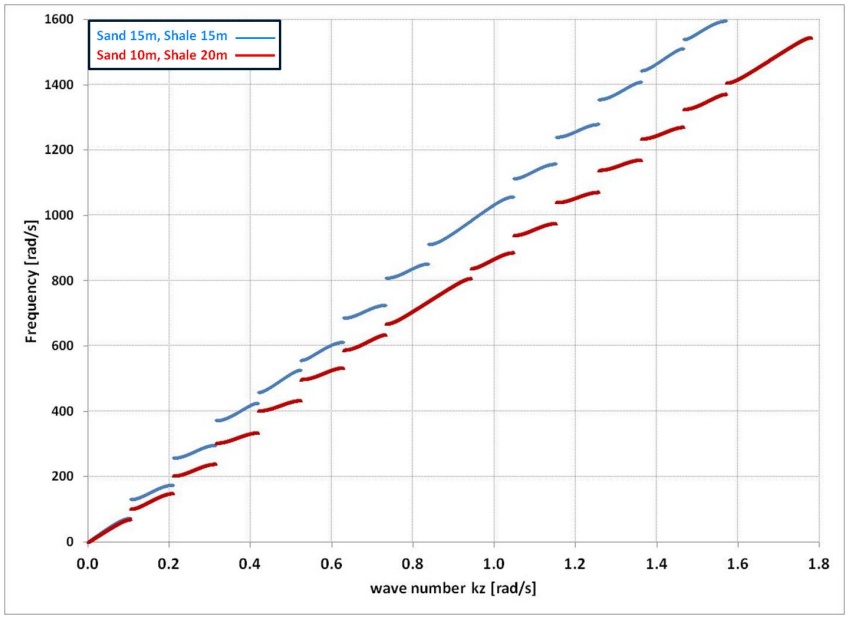

Figure 2.8: Dispersion relationship for variable constituent thickness, physical properties are shown in Table 2.1. The blue color is for a sand and shale thickness of 15m and 15m respectively. Red color is for sand and shale thickness of 10m and 20m respectively.

As mentioned before, the factors that affect the stop-band width are the velocity, density and thickness of the constituents. The analysis below is divided into three parts. In the first part, the behavior of the gap-width when the thickness of the layers changes is described. In the second part the behavior of the gap with change in V_s only is described. In the third part the change in density (ρ) only is described. Similar analysis was obtained by Rich (2006) using the P-wave dispersion relationship and P-impedance changes.

Figure 2.9 shows the stop-band width of the first four Brillouin zones as a function of the thickness of layers one and two. The parameters used in this experiment are shown at the top of the figure, allowing the thickness d_1 and d_2 to varies from 5% to

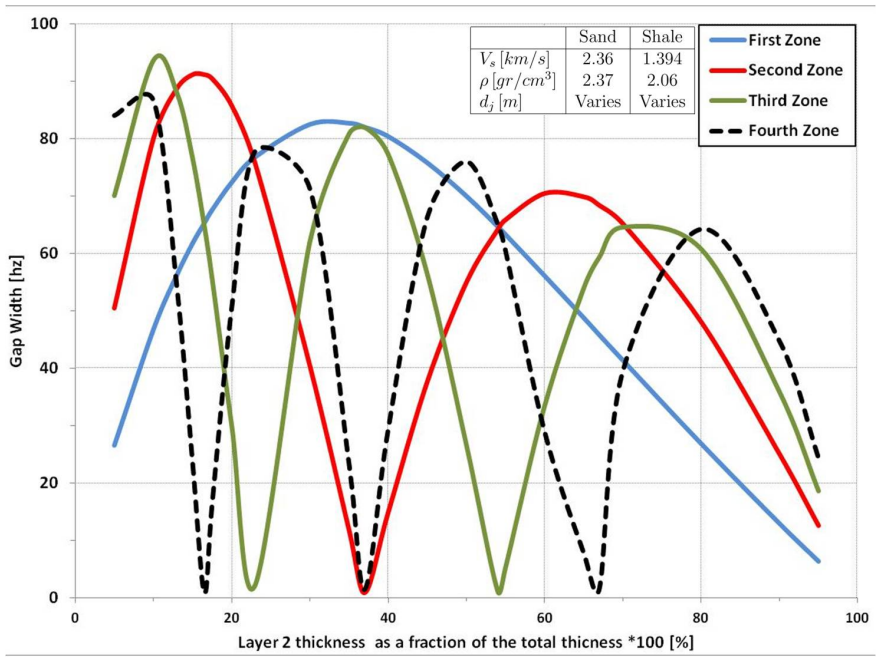

Figure 2.9: Gap or stop-band width as a function of changes in the thickness of layer two. The total thickness $d = d_1 + d_2$ is kept constant, $d = 30$m.

95% of the total thickness d with the constraint that the total thickness, $d = d_1 + d_2$, is kept constant at 30m. This experiment shows that the stop-band width for Brillouin zones two, three, and four disappears at certain values of d_2. On the other hand the stop-bands width for the first Brillouin zone has a maximum when $d_2 = 0.32d$. It is also observed that the higher the number of the Brillouin zone is, the faster the variability of the stop-band width is.

Figure 2.10 shows how the stop-band width changes when the S-velocity, density and S-impedance of the layer changes. The first case to consider is when the stop-band width changes when the variation of the shear modulus (μ), to ease the analysis, the value of μ_2 of the second layer is a percentage of the shear modulus of layer 1, and the density of both media have the same value as it is shown in the parameter table

at the top of this panel. The figure shows that for some values of V_{s2} the stop-band is not present. One special case is when $V_{s1} = V_{s1}$, in this case, all the stop-band widths are zeros because there are no boundaries between layers, since both of them have the same shear modulus and the medium is considered one layer. The first and second Brillouin zones do not show any other value of the V_{s2} where the stop band width is zero as opposed to the fifth Brillouin zone in which the stop-band disappears at values of $V_{s2} = .5V_{s1}$ and $V_{s2} = 1.33V_{s1}$. The fourth Brillouin zone shows only one value of V_{s2} where this width is zero ($V_{s2} = .67V_{s1}$). All of these observations support the conclusion that higher Brillouin zone numbers exhibit more variation of the stop-band width when the velocity changes are expected.

The middle panel of Figure 2.10 shows the variation of the stop-band width with the changes of ρ_2. To ease the analysis, the value of density for the second layer (ρ_2) is a percentage of the density of layer 1 (ρ_1). This figure shows that the stop-band width increases when the value ρ_2 increases or decreases, having the reference value of ρ_1. This observation is valid for first, second, fourth, and fifth Brillouin zones. The width of the third Brillouin zone is zero for all the values of the ρ_2. This is due to the particular values of velocity and density chosen for this example. In addition the value of zero stop-band width when $\rho_1 = \rho_2$ is not distinguished between layers and the medium is considered one layer.

The bottom panel of Figure 2.10 shows the variability of gap width with the change of S-impedance. The S-impedance is defined as $I_s = \rho V_s$ and to ease the analysis, the value of I_{s2} varies from 50% to 150% of I_{s1}. This case is more realistic

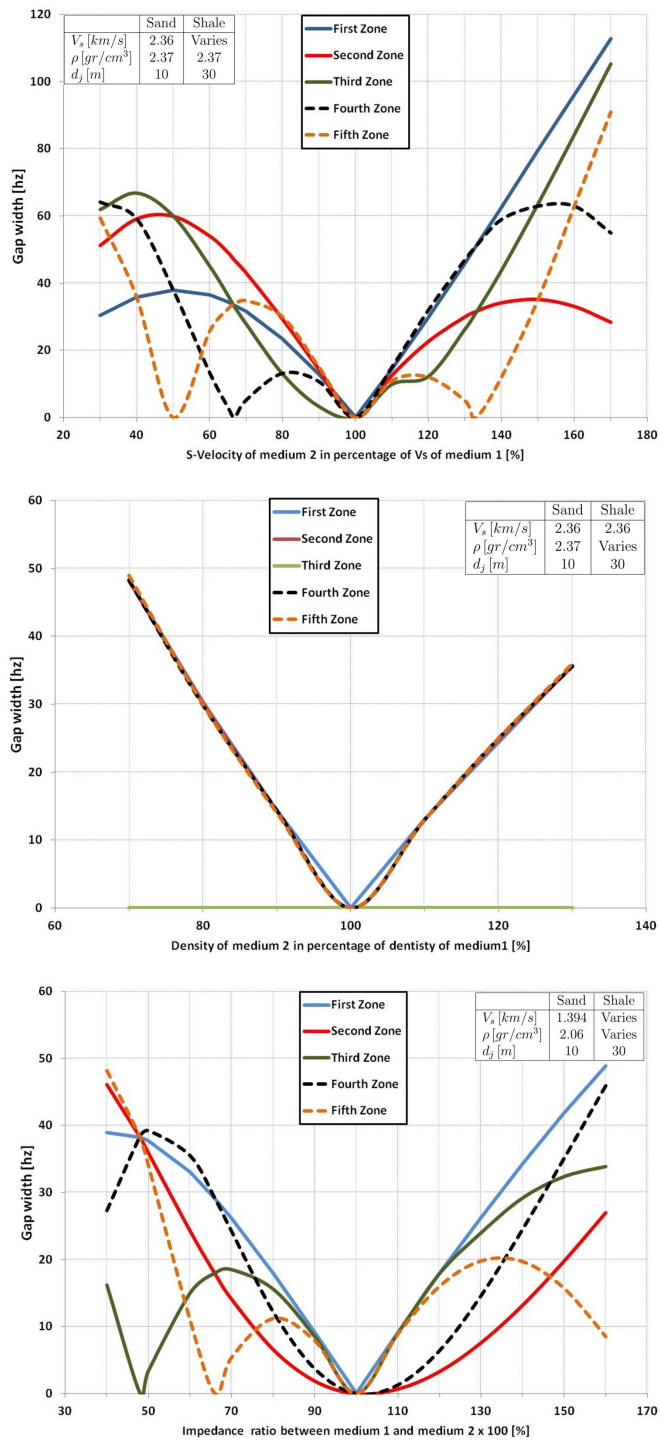

Figure 2.10: Gap or stop-band width as a function of changes in the physical properties (V_{s2}, ρ_2) and impedance $(I_s = V_{s2}\rho_2)$. Top panel shows the gap width as a function of changes of V_{s2}. Middle panel shows the gap width as a function of changes in density (ρ_2). Bottom panel shows the gap width as a function of changes in the impedance of the layer 2 with respect to layer 1. The parameters used in computation are shown at the top of each panel.

compared with the previous two cases, since the change in V_s always has an implicit change in shear modulus (μ) and/or density. In order to account for these simultaneous changes, the sand V_p-V_s and ρ-V_p relationships derived by Castagna *et al.* (1993) are used. These relationships are shown below:

$$\begin{aligned} V_s(km/s) =& .8042V_p - .8559 \\ \rho =& -.115V_p^2 + .261V_p + 1.515 \end{aligned} \tag{2.15}$$

The bottom panel of Figure 2.10 shows the function of the stop-band width with the change of I_s. It can be observed that the variation in impedance captures the behavior of changes in both ρ and V_s. This figure shows that the gap disappeared for Brillouin zones three and five. On the other hand, the gap-width increases for Brillouin zones one, two, and four in all the range of I_s.

2.4 Dispersion of S_h- waves traveling at any angle of propagation

So far the description of the S_h-wave has been done when $k_y = 0$. This mean that the wave propagates perpendicular to the layering. In order to study the S_h-wave propagating at any angle, $k_y \neq 0$ and the angle of propagation is given by $\alpha = \tan^{-1}(k_z/k_y)$. In this case the values of k_z that obey equation 2.8 for a given ω and k_y will give the dispersion relationship. Examples of this solution are given in

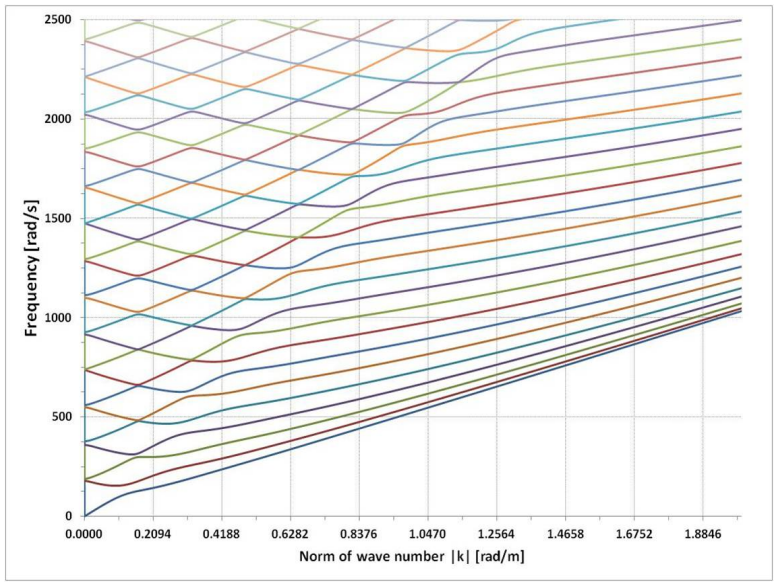

Figure 2.11: Dispersion relationships as a function of the norm of $\mathbf{k}$ for a S_h-wave traveling at $50°$ from the vertical axis z.

Figure 2.11. Notice that this picture does not show the periodicity of the medium anymore as it was shown for the case of $k_y = 0$.

Helbig (1984) suggested a different way of representing the dispersion relationship for this general case by plotting lines of constant frequency in the k_y-k_z plane. This representation is helpful for computation, since it is enough to compute the dispersion relationship for the first Brillouin zone at the desired frequency and then unfold them to the real position in a different Brillouin zone. This property was demonstrated by Brillouin (1946) and it is equivalent to the extended representation, explained in Figure 2.2. One example on how the values of $\omega(k_z, k_y)$ unfold to the second Brillouin zone is shown in Figure 2.12.

Figure 2.12 also shows the dispersion relationship in the case that the medium is isotropic (bottom centered panel). Comparing Figures 2.12.b and 2.12.c, it can be

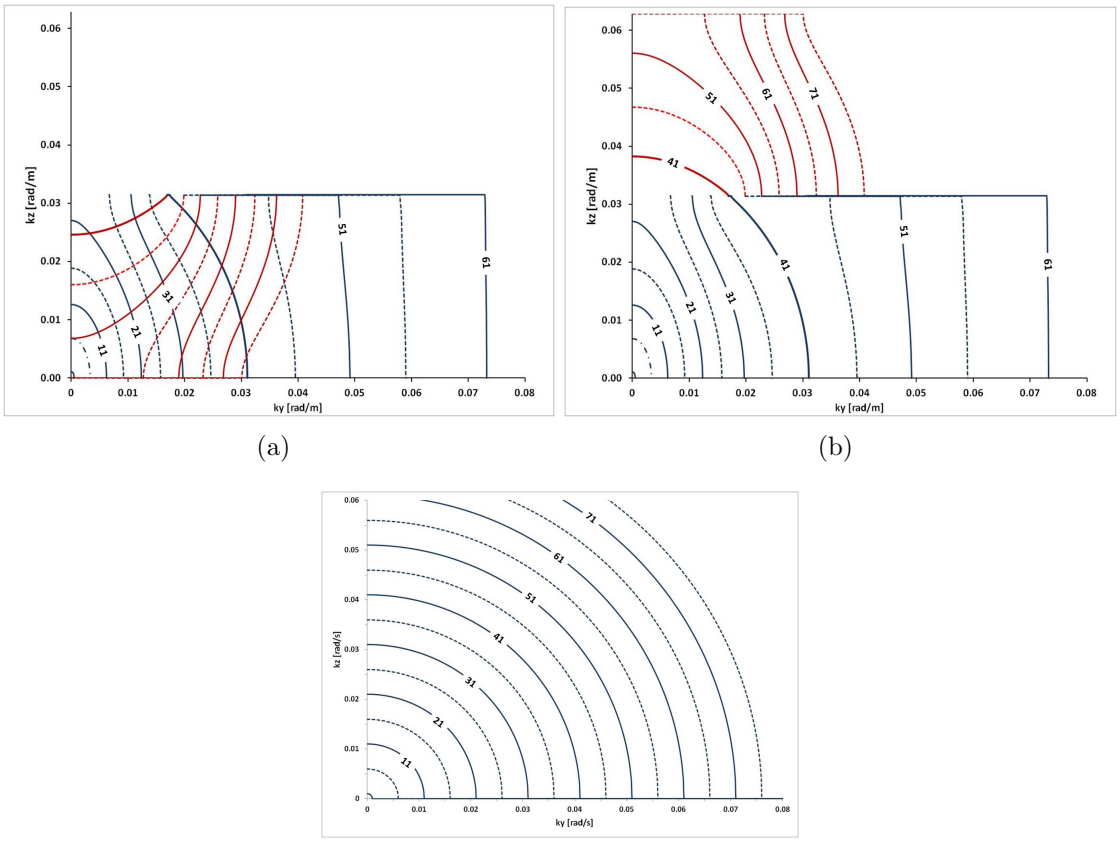

(a) (b)

(c)

Figure 2.12: Dispersion relationship for S_h-wave traveling at incidence angles from $0°$ to $90°$. Panel a) is the representation using reduced diagram (left top). Panel b) is the representation using the extended diagram (top right) and panel c) is the representation of dispersion relationship for isotropic medium(bottom center). Number inside the curve shows the frequency values.

seen that this periodic medium exhibits anisotropic behavior, since the contour lines do not follow an ellipse-shape as shown by Figure 2.12.c. In addition to this, there are some disconnected contour lines, as in examples where $\omega = 26hz, 31hz$, and $36hz$. This effect is evidence for the existence of stop-bands, since there are no vertical wavenumber (k_z) for these frequencies. Figure 2.13 shows the dispersion relationship in the k_z-k_y plane for constituent thickness equal to 50m ($d = d_1 + d_2 = 100m$) with more detail and a bigger range of frequencies from 1hz to 176hz. In this figure

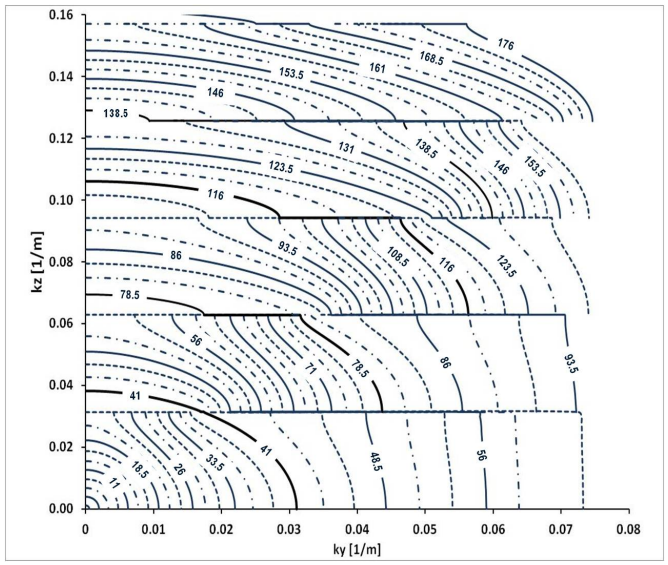

Figure 2.13: Extended representation of the dispersion relationship for S_h-wave traveling at angles of incidence from $0°$ to $90°$. Contour lines are every 2.5hz starting from 1hz, the number inside the curve shows the frequency values.

the boundaries of the Brillouin zones are also more evident. Rich (2006) shows the Sh-wave dispersion relationship in k_y-k_z for the same set of elastic parameter but for constituent thickness equal to 1m (medium period, d=2m). In general, Rich's and this study's dispersion relationships are similar, and they change only in scale of the axes. This is due to the difference in the order of magnitude of d.

The representation of the dispersion relationship in the k_y-k_z plane is also useful for computing the phase and group velocity of S_h-wave traveling at any angle, α, from the vertical. In order to compute the phase velocity, a line that represents a vector $\mathbf{k}$ in the plane k_y-k_z is necessary. This vector has a starting point at the origin $(k_y = 0, k_z = 0)$ and an end point at any point (k_y, k_z) that obeys $\tan(\alpha) = k_y/k_z$. The magnitude of the phase velocity would be $\omega/|\mathbf{k}|$. In order to compute the group

velocity, a vector perpendicular to a given frequency contour is needed, the group velocity at this point is equal to $d\omega/|d\mathbf{k}|$.

Another advantage of the k_y-k_z plane representation is the computation of the dispersion relationship for a S_h-wave traveling at any angle α. This dispersion relationship can be obtained by drawing a line at the desired angle, α. This angle is measured from the axis k_z. The values of $\omega(k_y, k_z)$ that intercept this straight line are the values of the $\omega(k_y, k_z)$ of the dispersion relationship at this α angle. Figure 2.14 shows these dispersion relation for different angles of propagation from the vertical for medium with parameters shown in Table 2.1 and constituent thicknesses ($d_j = 50m$). Rich (2006) computed this dispersion relationship for different angles using constituent thicknesses of 1m (d_j=$1m$).

Figure 2.14 also shows that wave propagation at different angles has the same characteristics as if traveling perpendicular to the layering. Both cases exhibit stop-bands, and the location of this stop-bands is proportional to the Brillouin zone width ($n\pi/d$). This proportional constant, n, depends on the angle α at which the wave field propagates.

It was stated in Section 2.3.4 that the stop-band width is a function of the thickness and S-impedance of the layer. Figure 2.14 shows that the stop-band width is also a function of propagation angle. Figure 2.15 shows the stop-band as a function of the S_h-wave propagation angle. The most interesting feature in this figure is that the stop-bands disappeared at an angle of 28°. This absence of stop-bands occurs when the line, defined by the angle of propagation, passes through points where frequency

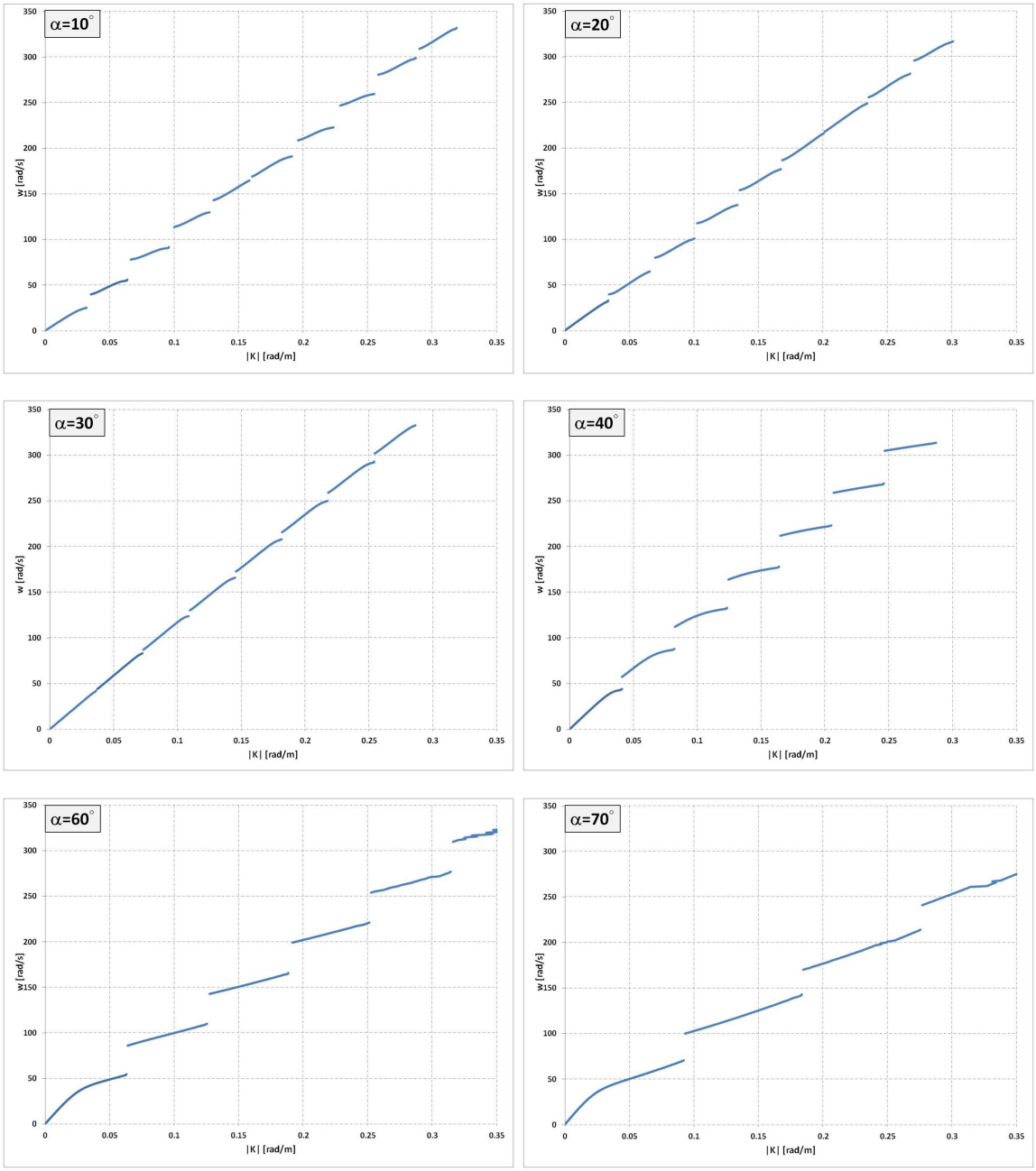

Figure 2.14: Extended diagram for the dispersion relationship for S_h-waves propagating at different angles. The propagation angle value, α, is shown at the top of each panel. This angle is measured from the vertical axis.

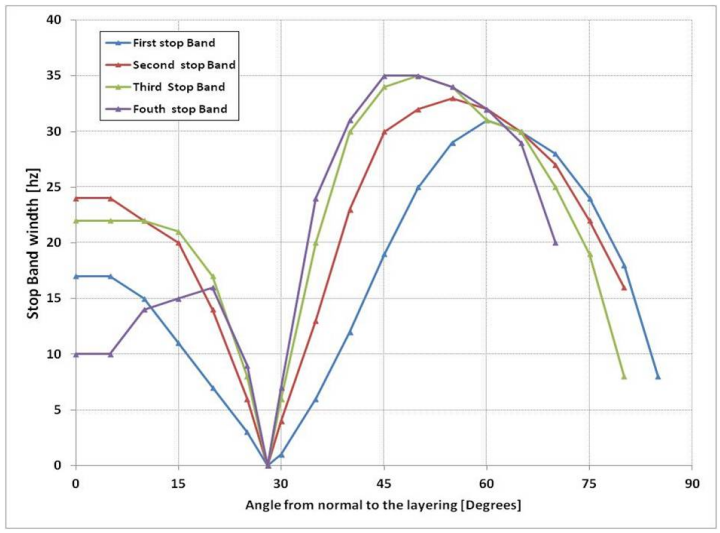

Figure 2.15: Stop-band width as function of the S_h-wave propagation angle for the first four Brillouin zones.

contours are continuous across Brillouin zones (Rich, 2006). Rich (2006) made the same simulation shown in figure 2.15 but using different constituent layer thicknesses (d_j=1m)

Comparing Figure 2.15 with the one shown in Rich (2006), it can be concluded that this critical angle is not a function of the layer thickness, since both studies shown the same critical angle value. The layer thicknesses d_j in Rich(2006) and this study are 1m and 50m respectively.

Other important observation in Figure 2.14 is the behavior of the fourth stop-band when compared to the other stop-bands. This stop-band starts to increase when the propagation angle increases from 0° to 20° as opposed to the other stop-bands. This can be explained by the high variability of the higher Brillouin zone number with the impedance values shown in Figure 2.10.

Figure 2.16 shows how this critical angle is function of the layers S-impedance. To address the change on S-impedance, the methodology described by equation 2.15 is used. This figure shows that the critical angle is present in the medium as long as there is a S-impedance contrast between constituents. The zero value of critical angle correspond when the two layers has the same S-impedance.

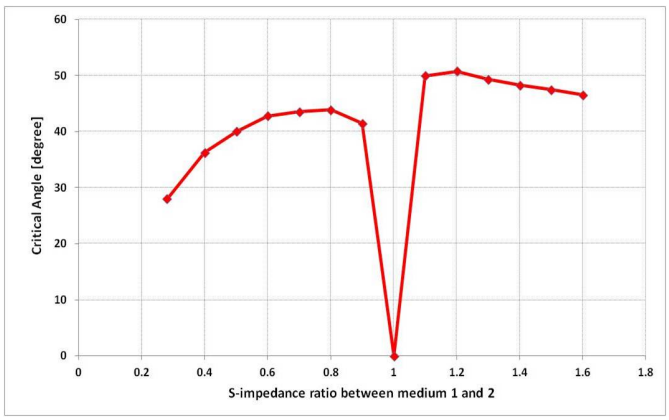

Figure 2.16: S_h-critical angle as a function of the S-impedance ratio between of the layer 1 and 2.

2.5 Dependence of the anisotropic coefficient as a function of the frequency

Once the dispersion relationship is obtained for every frequency value, the anisotropic coefficient can be computed with the equation (Chesnokov *et al.*, 2001):

$$Anisotropic\_Coeff = \frac{V_{sh}^{Max} - V_{sh}^{Min}}{V_{sh}^{Max}} \tag{2.16}$$

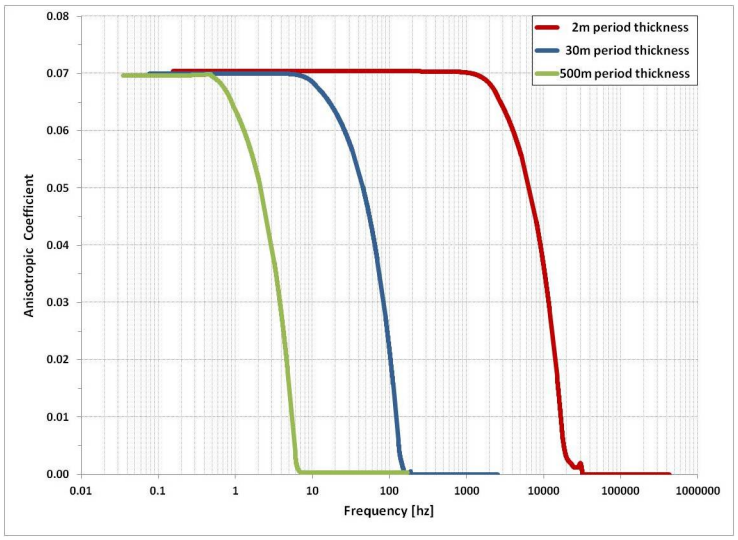

Figure 2.17: Anisotropic coefficient as a function of the frequency for different period thicknesses.

Figure 2.17 shows the relationship of the anisotropic coefficient with the frequency in a media with physical properties shown in Table 2.1 and different period thicknesses. This figure shows that the maximum anisotropic value is 7%. The frequencies at which this value is reached depend on the period thickness of the medium. For instance, for a medium with period equal 30m, the so called long-wave approximation is located between 0hz and 10hz.

On the other hand, the value of the anisotropic coefficient is zero when the frequency is higher than 110hz for the 30m period thickness medium. In this case the wave is propagating in the Ray Theory regime, i.e. the wavelength is much less than the period of the medium.

2.6 S_h-wave synthetic seismograph in layered periodic medium

In this section a synthetic seismograph is computed to understand the effect of the dispersion relationship when a S_h-wave is passes through a periodic medium. This seismograph is obtained using the Green's Function formulation and the function $\omega(k)$ that was discussed in previous sections. This methodology is explained in Rich (2006) and it is repeated here with a small modification in order to be able to compute incidence angle seismograph gather.

In general, an inhomogeneous differential equation has the form:

$$Lu(\mathbf{r}) = p(\mathbf{r}) \tag{2.17}$$

where L is a linear differential operator, that for the standard wave equation, has the form $\nabla^2 - \frac{1}{v^2}\frac{\partial^2}{\partial t^2}$. The solution to the homogeneous Equation of 2.17 is:

$$LG(\mathbf{r}, \mathbf{r}') = \delta(\mathbf{r} - \mathbf{r}') \tag{2.18}$$

where G is the Green's Function where the physical interpretation is the response of the medium to an impulse source (Aki and Richards, 1980). If the Green's Function

is known, then the solution to the inhomogeneous equation is given by:

$$u(\mathbf{r}) = \int G(\mathbf{r}, \mathbf{r}')p(\mathbf{r}')d\mathbf{r}' \tag{2.19}$$

Considering the solution to the standard wave equation in the frequency domain of the form:

$$G(\mathbf{r}, \mathbf{r}') = e^{-ik(\omega)\|\mathbf{r}-\mathbf{r}'\|} \tag{2.20}$$

where $k(\omega)$ is the inverse of the dispersion relationship $\omega(k)$ and $\|\mathbf{r}-\mathbf{r}'\|$ is the distance from the point source to the place where the measurement is taken. Applying the Fourier transform to equation 2.19, using equation 2.20 and considering point source at $\mathbf{r}_o$ equal to $p(\mathbf{r}', \omega) = p(\omega)\delta(\mathbf{r}' - \mathbf{r}_o)$. The following equation can be derived:

$$\begin{aligned} u(\mathbf{r}, \omega) = &\int G(\mathbf{r}, \mathbf{r}', \omega)p(\omega)\delta(\mathbf{r}' - \mathbf{r}_o)d\mathbf{r}' \\ =&G(\mathbf{r}, \mathbf{r}_o, \omega)p(\omega) \\ =&p(\omega)e^{-ik(\omega)\|\mathbf{r}-\mathbf{r}_o\|} \end{aligned} \tag{2.21}$$

Equation 2.21 shows that the phase shift of the displacement produce by the wavefield recorded at the point $\mathbf{r}$ is given by the distance between the source point and the point where the wavefield is recorded and the frequency $\omega(k)$. This $\omega(k)$ is the dispersion relationship already computed in the previous section which is a function of k_z, k_y and α ($\omega = f(k_y, k_z, \alpha)$). The displacement at distance $\mathbf{r}$ from the origin is the inverse Fourier transform of equation 2.21.

To compute the seismograph, the following steps were used. Step 1) Select the propagation angle α and compute the $k(w, k_y, k_z, \alpha)$ for a given model, for example dispersion relationships shown in Figure 2.14. Step 2) Define the source pulse in the time domain. Step 3) Perform a Fourier transform of the pulse. Step 4) Multiply each frequency component by the corresponding phase shift $e^{ik(k_z,k_y,\omega,\alpha,)d_o}$, where $d_o = |\mathbf{r} - \mathbf{r}_o|$ is the distance from the source position to the detector position and α is the wave incident angle measured from the vertical axis. Finally step 5) Perform the inverse Fourier transform. Figure 2.18.a shows these steps in a flow to compute a synthetic seismograph.

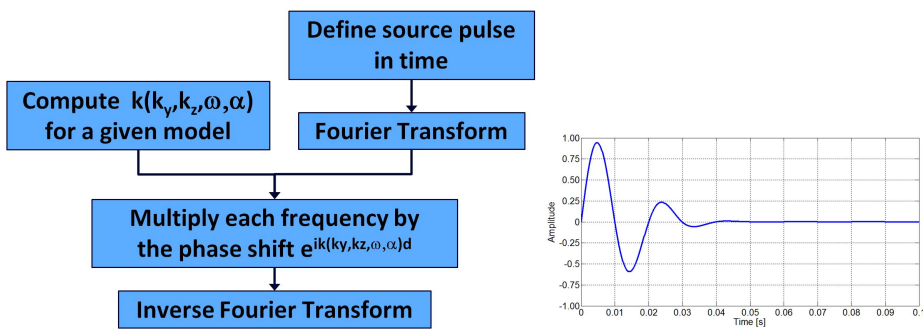

(a) (b)

Figure 2.18: Synthetic computation seismograph flow. a) Steps for computing synthetic seismograph. b) Source wavelet used in the computation.

Seismographs were computed for the model showed in Table 2.1. The source pulse or wavelet used was a Gaussian windowed sign given by the equation below:

$$p(t) = \sin(\omega_o t) e^{\frac{-2\omega_o^2 t^2}{n^2}} \tag{2.22}$$

where $\omega_0 = 2\pi f_o$ is the center frequency and n is the number of cycles. For these

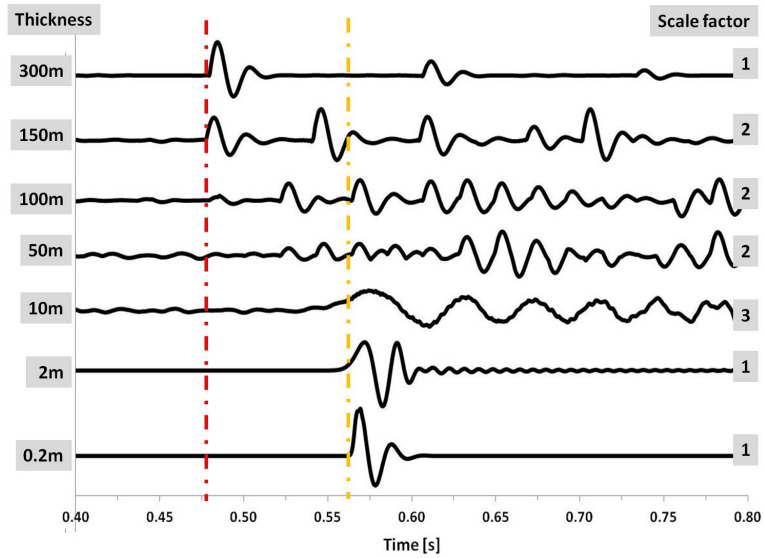

Figure 2.19: S_h-seismographs for variable medium period thickness. The value of the thickness is shown on the left of each seismograph. The vertical lines are the ray theory (red) and the effective media(yellow) time predictions for the 300m and 0.2m period thicknesses respectively. Number in the right hand side are the scaler factor applied to seismograph.

simulation the values used were $f_o = 50$hz and $n = 9$, the source wavelet is shown in Figure 2.18.b.

In order to compute the seismographs, the pulse is propagated over the distance of a 500 meters measured perpendicular to the layering. The thickness of the constituents layer had the same value for each computation ($d_1 = d_2$) but the periods were varied from 0.2m to 300m as it is shown in Figure 2.19. The same range of layer thickness were used by Rich (2006). In his study, he computed the S_h-wave propagating parallel and perpendicular to the layering.

Figure 2.19 shows the range of time and layer thickness where the Ray Theory and the Effective Media Theory are in effect. The seismograph with a period thickness of

300m shows the first reflection at 0.478s which corresponds to the total travel time of the S_h-wave through each individual layer (Ray Theory) and the subsequent picks are the energy bouncing in the faster layer. The energy bouncing from the slower layer would come 0.574s after the first arrival, since it takes 0.287s to go up and return in 0.287s. When the thickness of the period starts to get smaller there is more interference of this reflections until all the return reflections interfere constructively and the medium starts to behave as an effective medium.

In order to display the seismic traces in Figure 2.19, a scaler multiply factor was applied; this scaler value is shown on the right-hand side. Figure 2.19 shows a decrease in the amplitude accompanied by a change in frequency content at the transition between these two layer thickness values. This decrease in amplitude is associated with the presence of stop-bands in the frequency range of the source wavelet. The periodic medium acts as a filter for the input wavelet, transmitting selected frequencies in the finite-bandwidth wavelet and reflecting back other frequencies. This tuning effect contributes to the change in the frequency content of the received signal. This effect was shown experimentally by Marion *et al.* (1992).

Chapter 3

P- and $\mathbf{S_V}$-wave solution

3.1 Introduction

In this chapter the P- and S_v-wave propagating through a periodic medium is described and quantified. The dispersion relationship for these two wavefields are found using the same methodology used by Rich (2006).

3.2 P- and $\mathbf{S_v}$-wave solution

In chapter one, it was shown P- and S_v-wave is a solution of the wave equation 1.2 where the wave is propagating along the plane (y-z). The P-wave's displacement is along the propagation axes and the Sv-wave's displacement is perpendicular to the propagation axis. For this type of displacement the scalar and vector potential

choices are:

$$
\begin{aligned}
\phi =& f_j\left(z\right) e^{i(k_z z + k_y y - wt)}, \\
\psi_x =& g_j\left(z\right) e^{i(k_z z + k_y y - wt)} \\
\psi_y =& 0 \\
\psi_z =& 0
\end{aligned}
\tag{3.1}
$$

where $x_1 = x, x_2 = y, x_3 = z, k_z$ and k_y are the z and y components of the wave number vector $\boldsymbol{k}$ such that $k_z = |\boldsymbol{k}| cos\left(\theta\right)$ and $k_y = |\boldsymbol{k}| sin\left(\theta\right)$. Here θ is the angle from the z-axis. The subscript j refers to the solution in the j^{th}layer. With this choice of potential $\boldsymbol{\psi}$ given by equation 3.1, equation 1.4 takes the following form:

$$
\begin{aligned}
\rho \frac{\partial^2 \phi}{\partial t^2} =& \left(\lambda + 2\mu\right) \frac{\partial^2 \phi}{\partial y^2} + \frac{\partial^2 \phi}{\partial z^2}, \\
\rho \frac{\partial^2 \psi_x}{\partial t^2} =& \mu \left(\frac{\partial^2 \psi_x}{\partial y^2} + \frac{\partial^2 \psi_x}{\partial z^2} \right)
\end{aligned}
\tag{3.2}
$$

Substituting equation 3.1 into equation 3.2, leads to following equations

$$
\begin{aligned}
\frac{\partial^2 f_j}{\partial z^2} + 2ik_z \frac{\partial f_j}{\partial z} + \left(\frac{w^2}{c_{lj}^2} - k_z^2 - k_y^2 \right) f_j =& 0 \\
\frac{\partial^2 g_j}{\partial z^2} + 2ik_z \frac{\partial g_j}{\partial z} + \left(\frac{w^2}{c_{tj}^2} - k_z^2 - k_y^2 \right) g_j =& 0
\end{aligned}
\tag{3.3}
$$

where $c_l^2 = \frac{\lambda + 2\mu}{\rho}$ and $c_t^2 = \frac{\mu}{\rho}$ are the isotropic compressional and shear wave velocities, respectively. The solution to equation 3.3 is given by (Sve, 1971; Rich, 2006):

$$
\begin{aligned}
f_j(z) =& A_j e^{-iz(k_z - \alpha_j)} + B_j e^{-iz(k_z + \alpha_j)} \\
g_j(z) =& C_j e^{-iz(k_z - \beta_j)} + D_j e^{-iz(k_z + \beta_j)}
\end{aligned}
\tag{3.4}
$$

with $\alpha_j = \sqrt{\frac{w^2}{c_{lj}^2} - k_y}$ and $\beta_j = \sqrt{\frac{w^2}{c_{tj}^2} - k_y}$ and A_j, B_j, C_j, and D_j are constants that have their respective values when the boundary conditions are met. These boundary conditions obey the Floquet's Theorem where $f_j(z)$ and $g_j(z)$ are periodic functions with a period d of the medium such that $f_j(z) = f_j(z+d)$ and $g_j(z) = g_j(z+d)$.

Substituting equations 3.4 and 3.1 into 1.3, the following equation for displacements u_z and u_y are derived:

$$\begin{aligned}
u_z =& \frac{\partial \phi}{\partial z} - \frac{\partial \psi_x}{\partial y} \\
u_z =& \left[i\alpha_j \left(A_j e^{iz\alpha_j} - B_j e^{-iz\alpha_j} \right) - ik_y \left(C_j e^{iz\beta_j} + D_j e^{-iz\beta_j} \right) \right] e^{i(k_y y - \omega t)} \\
u_y =& \frac{\partial \phi}{\partial y} + \frac{\partial \psi_x}{\partial z} \\
u_y =& \left[ik_y \left(A_j e^{iz\alpha_j} + B_j e^{-iz\alpha_j} \right) + i\beta_j \left(C_j e^{iz\beta_j} - D_j e^{-iz\beta_j} \right) \right] e^{i(k_y y - \omega t)}
\end{aligned} \tag{3.5}$$

and for stresses σ_{yz} and σ_{zz} are:

$$\begin{aligned}
\sigma_{ij} =& \lambda \delta_{ij} \frac{\partial u_k}{\partial x_k} + \mu \left(\frac{\partial u_i}{\partial x_j} + \frac{\partial u_j}{\partial x_i} \right) \\
\sigma_{zz} =& \lambda \left(\frac{\partial u_y}{\partial y} + \frac{\partial u_z}{\partial z} \right) + 2\mu \frac{\partial u_z}{\partial z} \\
\sigma_{yz} =& \mu \left(\frac{\partial u_y}{\partial z} + \frac{\partial u_z}{\partial y} \right)
\end{aligned} \tag{3.6}$$

In order to find the value for the constants A_j,B_j,C_j, and D_j in equations 3.5 and 3.6, boundary conditions must be met. The boundary conditions are that the amplitudes of the displacements and stresses must be continuous at the boundary

between any two layers. The Floquet Theorem is also applied at the boundary d_1 and d_2 of the two layer, this gives the following conditions:

$$
\begin{aligned}
u_z\left(0^-\right) =& u_z\left(0^+\right), \\
u_z\left(d_1\right) =& u_z\left(-d_2\right) e^{(ik_z d)}, \\
u_y\left(0^-\right) =& u_y\left(0^+\right), \\
u_y\left(d_1\right) =& u_y\left(-d_2\right) e^{(ik_z d)}, \\
\sigma_{zz}\left(0^-\right) =& \sigma_{zz}\left(0^+\right), \\
\sigma_{zz}\left(d_1\right) =& \sigma_{zz}\left(-d_2\right) e^{(ik_z d)}, \\
\sigma_{yz}\left(0^-\right) =& \sigma_{yz}\left(0^+\right), \\
\sigma_{yz}\left(d_1\right) =& \sigma_{yz}\left(-d_2\right) e^{(ik_z d)}, \\
d =& d_1 + d_2
\end{aligned}
\tag{3.7}
$$

Using the above boundary conditions gives eight equations with eight unknowns. The representation of this 8x8 matrix is given in equation 3.8, this matrix is representing by two 8x4 sub-matrices. The first 8x4 matrix is composed of columns one through four and the second 8x4 matrix is composed of the columns five through eight.

$$
\begin{pmatrix}
\alpha_1 & -\alpha_1 & -k_y & -k_y \\
k_y & k_y & \beta_1 & -\beta_1 \\
k_y^2-\beta_1^2 & k_y^2-\beta_1^2 & 2k_y\beta_1 & -2k_y\beta_1 \\
-2k_y\alpha_1 & 2k_y\alpha_1 & k_y^2-\beta_1^2 & k_y^2-\beta_1^2 \\
\alpha_1 E_1 e_1 & -\alpha_1 E_1\overline{e_1} & -k_y E_1 e_2 & -k_y E_1\overline{e_2} \\
k_y E_1 e_1 & k_y E_1\overline{e_1} & \beta_1 E_1 e_2 & -\beta_1 E_1\overline{e_2} \\
(k_y^2-\beta_1^2)E_1 e_1 & (k_y^2-\beta_1^2)E_1\overline{e_1} & 2k_y\beta_1 E_2 e_2 & -2k_y\beta_1 E_1\overline{e_2} \\
-2k_y\alpha_1 E_1 e_1 & 2k_y\alpha_1 E_1\overline{e_1} & (k_y^2-\beta_1^2)E_1 e_2 & (k_y^2-\beta_1^2)E_1\overline{e_2}
\end{pmatrix}
\tag{3.8}
$$

$$
\begin{pmatrix}
-\alpha_2 & \alpha_2 & k_y & k_y \\
-k_y & -k_y & -\beta_2 & \beta_2 \\
(\beta_2^2-k_y^2)\gamma & (\beta_2^2-k_y^2)\gamma & -2k_y\beta_2\gamma & 2k_y\beta_2\gamma \\
2k_y\alpha_2\gamma & -2k_y\alpha_2\gamma & (\beta_2^2-k_y^2)\gamma & (\beta_2^2-k_y^2)\gamma \\
-\alpha_2 E_2\overline{e_3} & \alpha_2 E_2 e_3 & k_y E_2\overline{e_4} & k_y E_2 e_4 \\
-k_y E_2\overline{e_3} & -k_y E_2 e_3 & -\beta_2 E_2\overline{e_4} & \beta_2 E_2 e_4 \\
(\beta_2^2-k_y^2)\gamma E_2\overline{e_3} & (\beta_2^2-k_y^2)\gamma E_2 e_3 & -2k_y\beta_2\gamma E_2\overline{e_4} & 2k_y\beta_2\gamma E_2 e_4 \\
2k_y\alpha_2\gamma E_2\overline{e_3} & -2k_y\alpha_2\gamma E_2 e_3 & (\beta_2^2-k_y^2)\gamma E_2\overline{e_4} & (\beta_2^2-k_y^2)\gamma E_2 e_4
\end{pmatrix}
\begin{pmatrix}
A_1 \\ B_1 \\ C1 \\ D_1 \\ A_2 \\ B_2 \\ C_2 \\ D_2
\end{pmatrix}
= 0
$$

In equation 3.8, the following notation is used (Sve, 1971):

$$
\begin{aligned}
E_1\overline{e_1} =& e^{-id_1(k_z+\alpha_1)}, \quad & E_1 e_1 =& e^{-id_1(k_z-\alpha_1)}, \\
E_1\overline{e_2} =& e^{-id_1(k_z+\beta_1)}, \quad & E_1 e_2 =& e^{-id_1(k_z-\beta_1)}, \\
E_2\overline{e_3} =& e^{id_2(k_z-\alpha_2)}, \quad & E_2 e_3 =& e^{id_2(k_z+\alpha_2)}, \\
E_2\overline{e_4} =& e^{id_2(k_z-\beta_2)}, \quad & E_2 e_4 =& e^{id_2(k_z+\beta_2)}, \\
\lambda_j k_y^2 + \alpha_j^2(\lambda+2\mu) =& \mu_j(\beta_j^2 - k_y^2), \quad & \gamma =& \frac{\mu_2}{\mu_1}
\end{aligned}
\tag{3.9}
$$

Equation 3.8 is different from the one reported by Rich (2006), specifically in those terms when the boundary condition is applied at d_1 and d_2. On the other hand, equation 3.8 is identical to the one reported by Sve (1971).

Equation 3.8 has a mathematical solution only if the determinant of the 8x8 matrix is zero. This determinant equal zero procedure gives a characteristic polynomial that is solved for k_z when the k_y and ω are given. The values of k_z, k_y, and ω that obey this characteristic polynomial define the P- and S_v-wave dispersion relationship. A $Matlab^{©}$ program was written to solve this determinant.

The propagation on the P- S_v-wave can be divided in propagation perpendicular to the layers and propagation along an angle; this angle is measure from vertical axis. When the propagation is perpendicular to the layer, $k_y = 0$ and the characteristic polynomial is solved for k_z for each ω value.

When the P- and S_v-wave propagates at angle (α), measured from the vertical axis, the wave number components, k_z and k_y, have the values $k_z = |\boldsymbol{k}|\cos(\alpha)$ and

$k_z = |\boldsymbol{k}| \sin(\alpha)$ respectively, where $|\boldsymbol{k}| = \sqrt{k_z^2 + k_y^2}$. In the next section the P- and S_v-wave dispersion relationship is analyzed for different propagation angles.

3.3 Dispersion of P- and S_v-waves traveling perpendicular to layering

The solution to equation 3.8 gives the dispersion relationship for P- and S_v-waves propagating in a periodic medium. In the case of perpendicular propagation to the layer bedding, the angle measured from the vertical axis, α, is equal to zero and from this $|\boldsymbol{k}| = k_z$. The determinant is solved numerically for the sand-shale model given in Table 2.1. Figure 3.1.a shows the solution to the equation. It can be seen that the solution contains the dispersion relationship for the P- and S_v-wave together. This is a consequence of the coupling of these two waves in the displacement equation when the Helmholtz' scalar and vector potentials are used in equation 3.5.

In order to decouple the P- and S_v-wave solution of Figure 3.1.a into the corresponding P- and S_v-dispersion relationships, the values of the A_1,A_2,B_1,B_2,C_1,C_2,D_1, and D_2 for each value of k_z and ω must be found. This procedure is equivalent to finding the eigenvector for the eigenvalue k_z. Once the eigenvector-vectors are found by the orthogonally property of these vectors, it can be known which k_z values correspond to P-wave and which ones correspond to S_v-waves. In this way, the two waves can be separated in to its corresponding dispersion relationships. This is shown in Figure 3.1.b and 3.1.c, respectively.

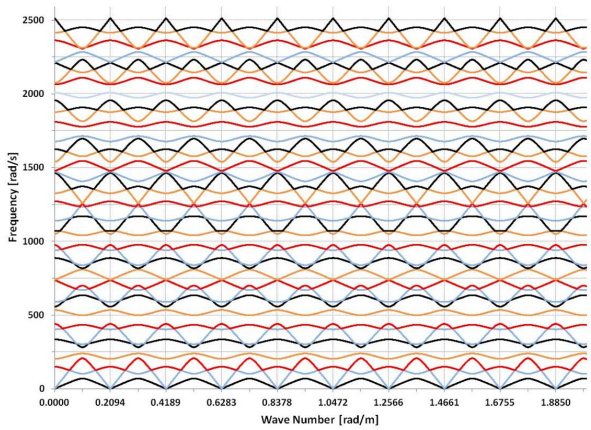

(a)

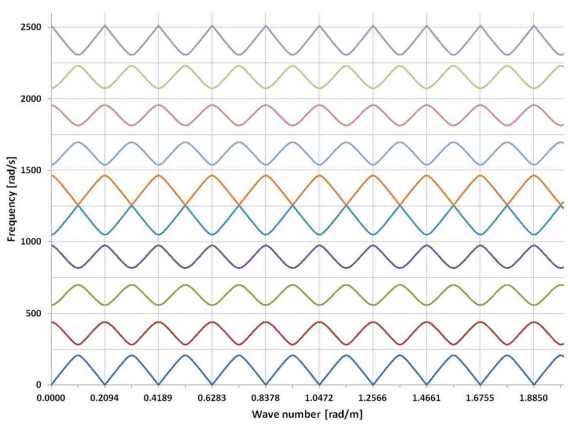

(b)

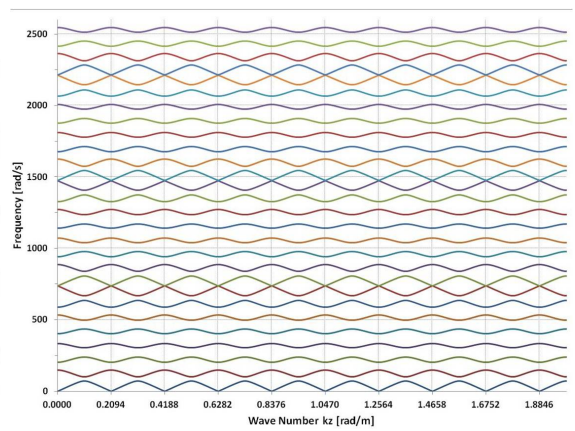

(c)

Figure 3.1: a) Solution to equation 3.8 solving for k_z using parameter of Table 2.1. b) Spectrum of V_p as a function of the wavenumber. c) Spectrum of V_s as a function of the wavenumber.

Figure 3.1 also shows that the P- and S_v-dispersion relationship are periodic with the period given by $2\pi/d$, as it was also the case for the S_h-wave shown in the previous chapter. This characteristic allows the Brillouin zone to be defined and the extended representation to be applied as it was done for the S_h-wave. Figure 3.2 shows the extended representation of dispersion relationship for P- and S_v-wave. This figure shows two features. The first feature is that the P- and S_v-wave shows stop-bands as

in the case of S_h-waves. The second feature is that the S_v-wave dispersion relationship has the same values as those derived for the S_h-wave case. This is true in the case of wave propagation perpendicular to the bedding but the two dispersion relationships are different for the case of wave propagation with an angle from the vertical axis ($\alpha \neq 0$).

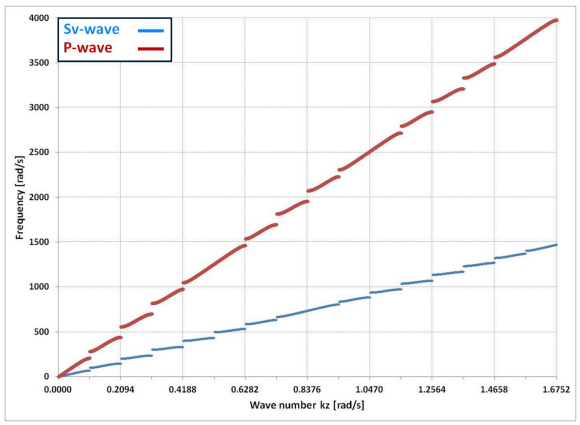

Figure 3.2: Extended representation of the P- and S_v-wave dispersion relationship.

3.3.1 P- and S_v-wave phase velocity as a function of frequency

One use of the extended representation of the dispersion relationship is to compute the phase velocity of the wave traveling in a period media. Figure 3.3 presents plots of the phase velocity as a function of the frequency (ω) using the model shown in Table 2.1. Both phase velocities plots exhibit a modulation behavior which is also present in the S_h-wave case. As shown in previous chapter this modulation is a function of the impedance and the thickness of the constituents.

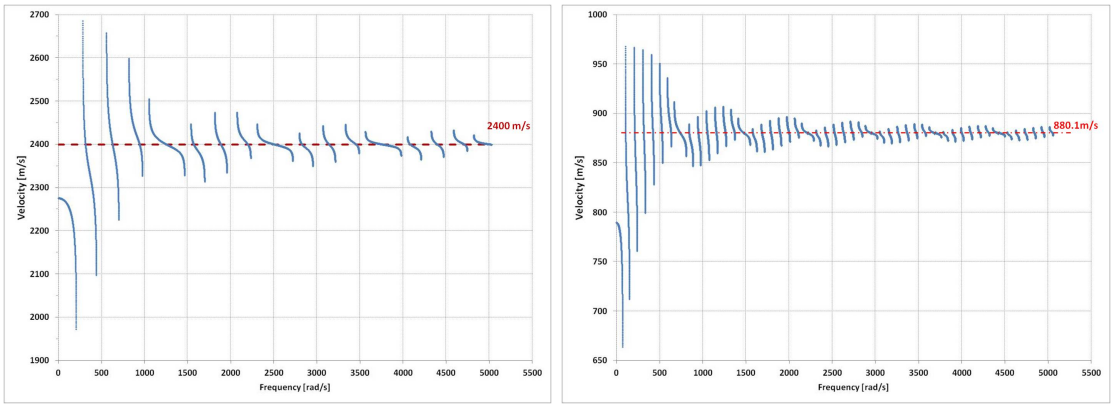

(a) (b)

Figure 3.3: Velocity as function of ω for P and S_v-waves. a) P-wave phase velocity and b) S_v-wave phase velocity. Line in red is the ray theory velocity.

3.3.2 P-wave phase velocity as a function of wavelength

Figure 3.4 shows the P-wave phase velocity as a function of the ratio between the wavelength and the thickness of the period of the medium ($\frac{\lambda}{d}$). This figure shows that the V_p phase velocity at large wavelengths compared with d, can be approximated as the velocity computed through the Effective Media Theory (green line in Figure 3.4). On the other hand, if the wavelength is much smaller than d the phase velocity can be approximate as the velocity computed by the Ray Theory (red line in Figure 3.4). These two theories explain how the medium behaves in the limit cases. When the wavelength is comparable with d ($\lambda \approx d$), a lot of dispersion effects take place, mainly due to scattering phenomena (Marion *et al.*, 1994). This is observed in Figure 3.4 when $0.1 > \frac{\lambda}{d} < 10$. The S_v-wave dispersion relationship is the same as the one found for the S_h-wave. This S_h-wave phase velocity is showed in figure 2.7

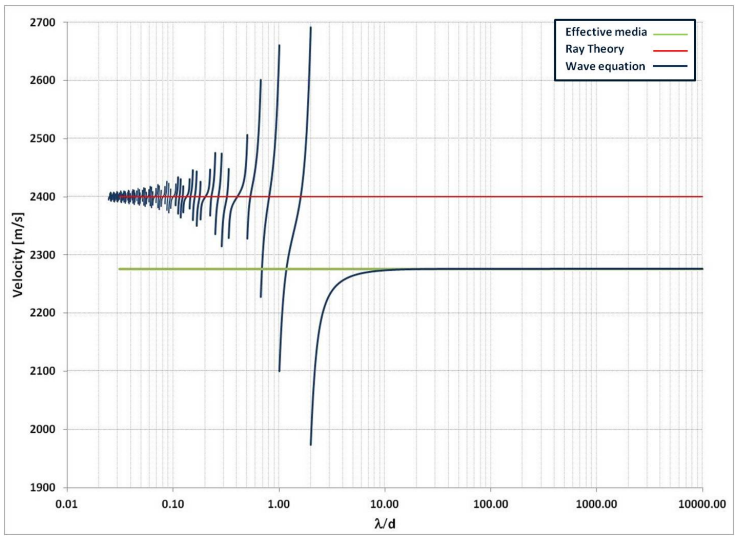

Figure 3.4: $\frac{\lambda}{d}$ vs. **P**-wave phase velocity with propagation normal to layers for alternating sand and shale medium. The green and red lines show the velocity computed by the Ray and Effective Media Theory respectively.

3.4 Dispersion of P- and $\mathbf{S_v}$-waves traveling at general propagation angles

Solving equation 3.8 for k_z and k_y gives the dispersion relationship for P- and S_v-waves traveling at any angle from the vertical axis. Since the P- and S_v waves are coupled, there are phenomena at the interface of each layer that involves more than one mode of propagation, for instance at each interface (boundary between layers), there are conversions from P to S_v modes and from S_v to P. Another effect is due to the angle of incidence of the wave, since critical refraction angle of propagation can be reached and in this case the waves travel along the interfaces.

In contrast from the S_h-wave case, the dispersion relationship for P- and S_v-wave does not have an analytical solution and the determinant of equation 3.8 has to be

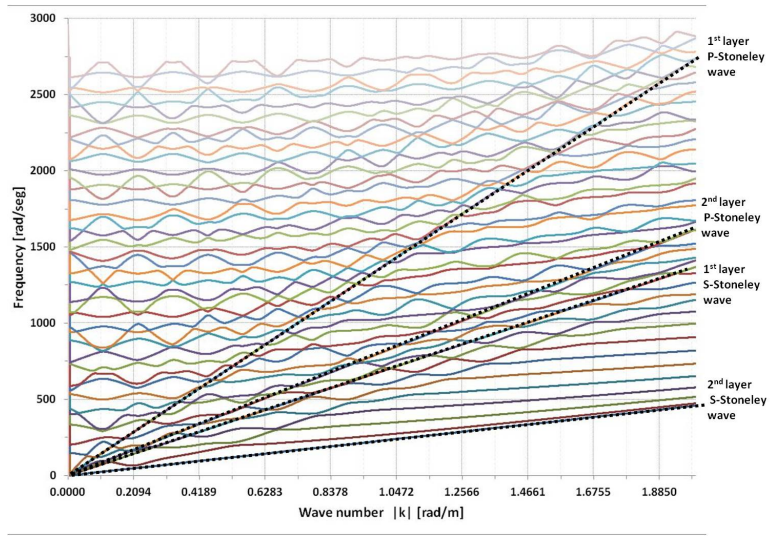

Figure 3.5: Dispersion relationship for P- and S_v-wave traveling at $20°$ measured from the perpendicular axis. Dash lines show the Stoneley waves phase velocity for each layer.

solved numerically. The dispersion relationship is plotted as a function of $|\mathbf{k}|$, where $|\mathbf{k}| = \sqrt{k_y^2 + k_z^2}$. Figure 3.5 shows this relationship for the P and S_v-waves using the model in Table 2.1. Wave propagation is at $\alpha = 20°$ measured from the vertical axis. This figure shows the different Stoneley phase waves velocities. Stoneley waves are waves that propagate along the interface (Sheriff, 1997). These velocities have the values $V_{pj}\sin(\alpha)$ and $V_{sj}\sin(\alpha)$, where j is the layer constituents number.

Figure 3.5 also shows that the dispersion curves are not periodic; however plotting this relationship in the k_y-k_z plane (Figure 3.6), it can be seen that the dispersion relationship follow, in certain ways, the behavior of the S_h-wave. However, due to the P- and S_v-wave coupling, extra computation has to be taken since the solution of equation 3.8 gives both values of k_{zp} and k_{zs} corresponding to each wave respectively. In order to decouple these two wave the values of the eight constants

(A_1,B_1,C_1,D_1,A_2,B_2,C_2, and D_2) for each value of $\omega(k_y, k_z)$ needs to be computed. This process is similar to finding the eigenvector of the solution for equation 3.8. An example of this process is shown in Figure 3.6, the model described in Table 2.1 is used in this simulation.

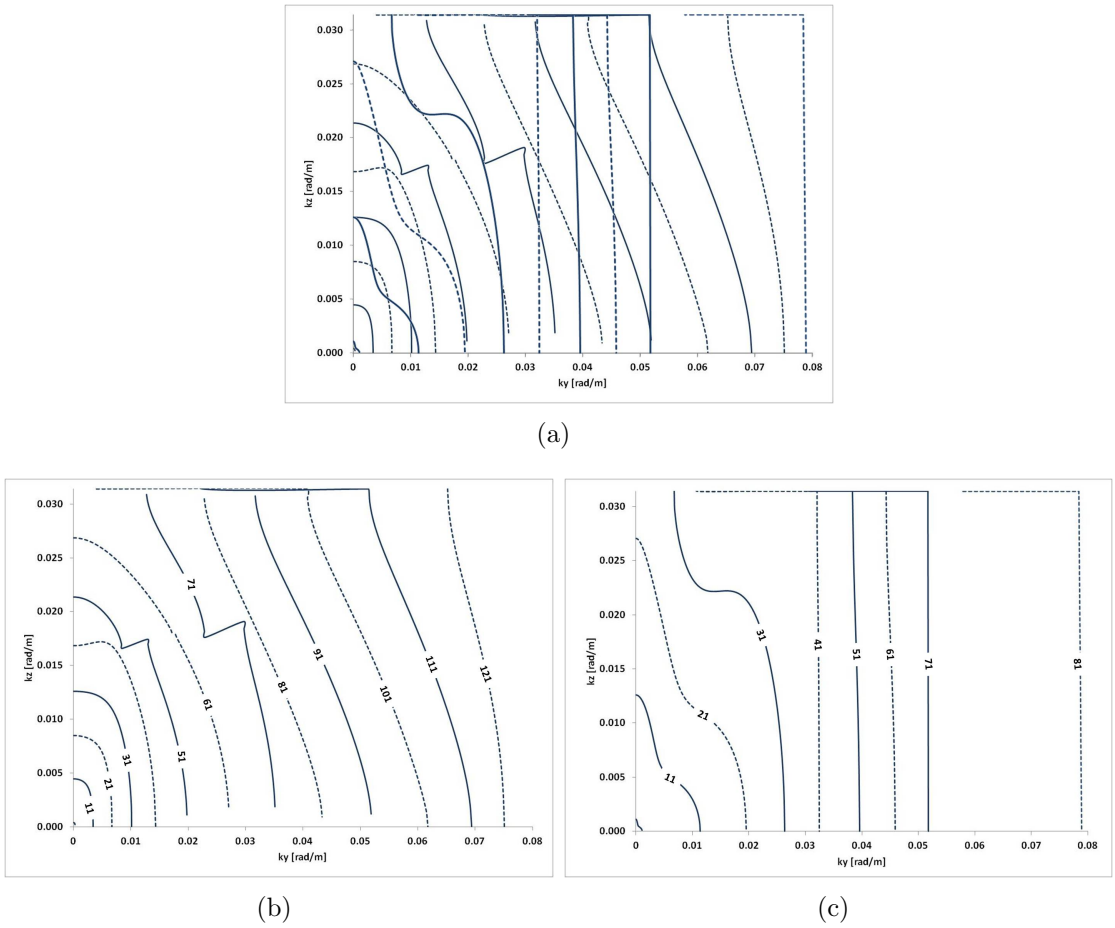

Figure 3.6: Representation of the P- and S_v-wave dispersion relationship in the k_y-k_z plane, contour lines are at constant ω. a) Complete solution of equation 3.8, b) decoupled P-wave dispersion relationship and c) decoupled S_v-wave dispersion relationship. Contour lines are every 10hz from1hz to 121hz, the number inside the curves shows the frequency values.

Figure 3.7 shows the dispersion relationship for the P and S_v-wave in more detailed after the decoupling is done. In this plot the real and the imaginary solutions

are shown. The imaginary values of the dispersion relationship correspond to inhomogeneous waves that travel along the interface and are attenuated away from the interface. The real values of the dispersion relationship describes the phase of the homogeneous waves, these waves do not attenuate when they pass through the interface (Aki and Richards, 1980). The wave propagation angle can be computed from Figure 3.6 using $\tan(\alpha) = (k_y/k_z)$. The boundary between the real and imaginary values of the dispersion relationship correspond to the critical angle and for the model of Table 2.1, this critical angle has a value of 30° and 16.5° for P and S_v-wave, respectively.

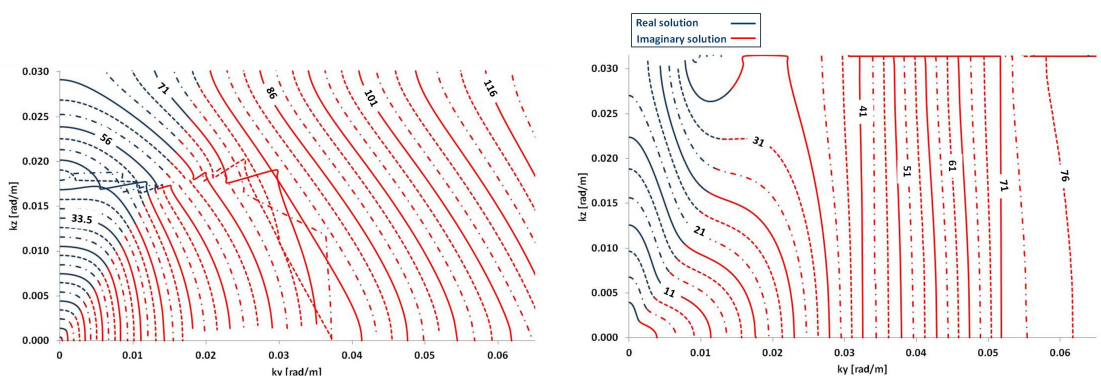

(a) (b)

Figure 3.7: Representation of the P- and S_v-wave dispersion relationship in the k_y-k_z plane for the first Brillouin zone, contour lines are at constant ω. a) P-wave dispersion relationship and b) S_v-wave dispersion relationship. Contour lines are every 2.5hz starting at 1hz, the number inside the curves shows the frequency values.

Figure 3.7 also shows that the P- and S_v-waves exhibit an anisotropic behavior because the dispersion relationship for both waves does not show a circular shape which is characteristic of isotropic media as it was shown in the previous chapter.

As in the S_h-wave case, P- and S_v-wave dispersion relationships also show a

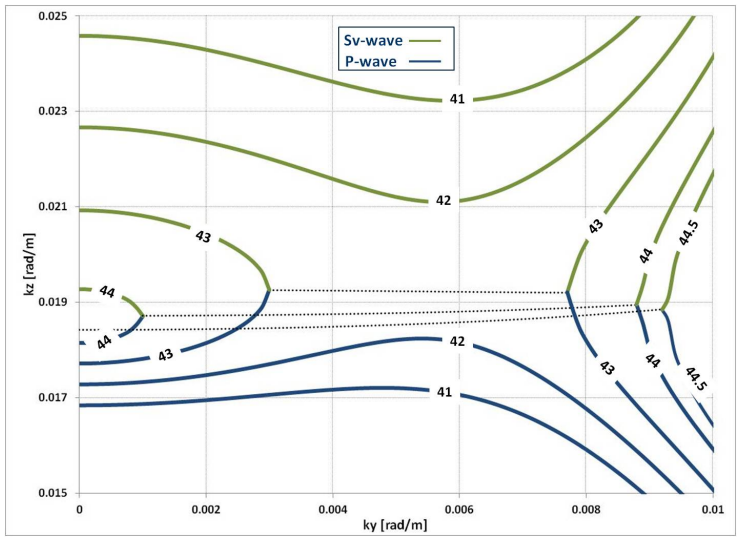

Figure 3.8: Dispersion relationship for P-wave in the k_y-k_z plane. Dash lines show the stop-bands for that specific frequency. Numbers inside the curves show their respectively frequency (ω) values.

periodic behavior and stop-bands at the boundary of the Brillouin zone when the waves travel at angles different from the perpendicular direction of the bedding ($\alpha \neq 0°$). However, a feature that differs from the S_h-wave is that the P- and S_v-wave dispersion relationships shows stop-bands inside the Brillouin zone. This happens when the phase of the P-wave is equal to the phase of S_v-wave. Figure 3.8 shows these stop-bands within the first P-wave Brillouin zone; the S_v-wave phase in this figure has not been unfolded to its real position since the reduced representation is used. These values of S_v-dispersion relationship belong to the second S_v-wave Brillouin zone. Figure 3.8 also shows that the width of this intra-Brillouin zone stop-bands is a function of the frequency and the angle of wave propagation. This phenomenon is also reported when acoustic phonons travel in super-lattices (Kato, 1997).

Conclusions

The purpose of this thesis was to provide a physical description of the waves traveling through an elastic periodic medium. P-, S_v-, and S_h-waves were analyzed using the methodology described by Sve (1971) and Rich (2006). For the case of P- and S_v-wave, an 8x8 determinant had to be solved numerically. For the S_h-wave case an equation for the dispersion relationship was found (see Appendix A in this thesis). The dispersion relationship for all the waves showed a periodic function with the period of $d = d_1 + d_2$ in the z-direction. This periodicity allowed the definition of Brillouin zone whose width was equal to π/d.

Depending on the wavelength, the wave propagation in periodic layered media show three regimes. If the wavelength (λ) is greater than 10 times the period of the medium (d), the wave treats the medium as an effective anisotropic one. This behavior is described by the Effective Media Theory. On the other hand, if the wavelength is less than 0.1 times the period of the medium (d), the wave travels through the medium as if the medium were isotropic. This behavior corresponds to the Ray Theory regime. In the region between 0.1 and 10 times the period of the medium (d) is the transition zone where the wave exhibits a lot of scattering

phenomena.

These regimes are also found when the wave frequency is allowed to vary. For instance for a medium with $d = 30$, the maximum anisotropic value is 7% and is reached at frequencies between 0hz and 10hz. This range corresponds to the long-wave approximation. On the other hand, the value anisotropic is zero when the frequency is higher than 110hz. In this case the wave is propagating in the ray theory regime, i.e. the wavelength is much less than the period of the medium.

In addition of the Brillouin zones, the dispersion relationship shows stop-bands for all waves: P,S_h and S_v. This stop-bands are defined as localized frequency zones where waves do not propagate. This stop-bands are found at the boundary of each Brillouin zone where the wave shows multiple reflections that do not allow the wave to propagate in this frequency range (Marion *et al.*, 1994). It was found that the width of these stop bands is a function of the propagation incidence angle, impedance contrast and layer thickness. It was also found that the higher the number of the Brillouin zones the more sensitive the stop-band width is to these factors.

Simulation on the Sh-wave propagating through a layered periodic medium showed the existence of a critical angle at which the stop-bands disappear for the S_h wave. This phenomenon appears at 28° for the model shown in Table 2.1. The absence of stop-bands happens when the angle of wave propagation coincides where the separation in frequency between Brillouin zones is minimum or close to zero (Rich 2006). Further simulation done in this thesis shown that the critical angle is not a function of the medium constituent thicknesses but it is a function of the constituent

impedance contrasts.

Beside the stop-band at the boundary of the Brillouin zone, the P- and S_v-waves exhibit stop-bands inside the Brillouin zones. This phenomenon could be explained as the multiple reflections presence at the boundary between layer due to the conversion of P-waves into S_v-waves or S_v-waves into P-waves. This phenomenon occurs when the phase of the P-wave is the same as the phase of the S_v-wave. It was shown that these stop-bands are a function of the wave frequency and the incident wave angle.

References

Aki, K., and Richards, P. G., 1980, *Quantitative Seismology Theory and Methods*, W. H. Freeman and Company.

Brillouin, L., 1946, *Wave Propagation in Periodic Structures*, McGraw-Hill Book Company, Inc.

Castagna, J. P., Batzle, M. L., and Kan, T. K., 1993, Rock physics - The link between rock properties and AVO response: Offset-dependent reflectivity - Theory and practice of AVO analysis: SEG, 135–171.

Chesnokov, E., Queen, J., Vichorev, A., Lynn, H., Hooper, J., Bayuk, I., Castagna, J., and Roy, B., 2001, Frequency dependent anisotropic: SEG Expanded Abstract, **20**(ANISOTROPY I).

Coe, A. L., Bonsence, D. W., Church, K. D., Flint, S. S., Howell, J. A., and Wilson, R. C. L., 2003, *The Sedimentary Record of Sea-level Change*, Cambridge University Press.

Helbig, K., 1984, Anisotropy and dispersion in periodically layered media: Geophysics, **49**(4) 364–373.

Kato, H., 1997, Acoustic SH phonons in superlattice with (111) interfaces: Journal of Acoustical Society of America, **101**(3) 1380–1387.

Lee, E. H., and Yang, W. H., 1973, On waves in a composite materials with periodic structure: SIAM Journal on Applied Mathematics, **25**(3) 492–499.

Marion, D., Mukerji, T., and Dvorkin, J., 1994, Scale effects on velocity dispersion: from ray to effective medium theories in stratified media: Geophysics, **59**(10) 1613–1619.

Mavko, G., Mikerji, T., and Dvorkin, J., 2003, *The Rock Physics Handbook*, Cambridge University Press.

Postma, G. W., 1955, Wave Propagation in a stratified medium: Geophysics, **20**(4) 780–806.

Rich, J., 2006, Quantitative Analysis of Material Contrast and Wave Propagation in a Periodic Layer Media, Ph.D. thesis, University of Oklahoma.

Rytov, S. M., 1956, Acoustical propeties of a thinly laminated medium: Soviet Physics Acoustics, **2** 68–80.

Sheriff, R., 1997, *Encyclopedic Dictionary of Exploration Geophysics*, The Society of Exploration Geophysicists.

Sun, C. T., Achenbach, J. D., and Herrmann, G., 1968, Continuum Theory for laminated medium: Journal of Applied Mechanics,Transactions of the ASME Series E, **90**(2) 467–475.

Sve, C., 1971, Time-harmonic wave traveling obliquely in a periodically laminated medium: Journal of Applied Mechanics,Transactions of the ASME Series E, **38**(2) 477–482.

Vernik, L., and Nur, A., 1996, Ultrasonic velocity and anisotropy of hydrocarbon source rocks: Geophysics, **57**(5) 727–735.

Wyllie, M. R. J., Gregory, A. R., and Gardner, L. W., 1956, Elastic wave velocities in heterogenous and porous media: Geophysics, **21** 41–70.

Appendix A

Computation of S_h-dispersion relationship

This appendix contains the derivation of equation 2.8. The starting point is equation 2.7, for convenience it is repeated below:

$$\begin{pmatrix} 1 & 1 & -1 & -1 \\ e^{-id_1(k_z+\beta_1)} & e^{-id_1(k_z-\beta_1)} & -e^{id_2(k_z+\beta_2)} & -e^{id_2(k_z-\beta_2)} \\ -\beta_1\mu_1 & \beta_1\mu_1 & \beta_2\mu_2 & -\beta_2\mu_2 \\ -\beta_1\mu_1 e^{-id_1(k_z+\beta_1)} & \beta_1\mu_1 e^{-id_1(k_z-\beta_1)} & \beta_2\mu_2 e^{id_2(k_z+\beta_2)} & -\beta_2\mu_2 e^{id_2(k_z-\beta_2)} \end{pmatrix} * \begin{pmatrix} E_1 \\ F_1 \\ E_2 \\ F_2 \end{pmatrix} = 0 \tag{A.1}$$

This equation only has solution when the determinant of the left matrix is equal to zero. This determinant is:

$$\left\| \begin{matrix} 1 & 1 & -1 & -1 \\ \overline{E}_1\overline{e}_1 & \overline{E}_1 e_1 & E_2 e_2 & -E_2\overline{e}_2 \\ -\beta_1\mu_1 & \beta_1\mu_1 & \beta_2\mu_2 & -\beta_2\mu_2 \\ -\beta_1\mu_1\overline{E}_1\overline{e}_1 & \beta_1\mu_1\overline{E}_1 e_1 & \beta_2\mu_2 E_2 e_2 & -\beta_2\mu_2 a E_2\overline{e}_2 \end{matrix} \right\| = 0 \tag{A.2}$$

where the below notation is used:

$$\begin{aligned} E_1 &= e^{id_1k_z}, & \overline{E}_1 &= e^{-id_1k_z} \\ e_1 &= e^{id_1\beta_1}, & \overline{e}_1 &= e^{-id_1\beta_1} \\ E_2 &= e^{id_2k_z}, & \overline{E}_2 &= e^{-id_2k_z} \\ e_2 &= e^{id_2\beta_2}, & \overline{e}_2 &= e^{-id_2\beta_2} \\ \beta_j &= \sqrt{\frac{w^2}{c_j^2} - k_y^2} \end{aligned}$$

j is the layer numbers and c_j is the each layer S-velocity.

Solving for the determinant of equation A.2, the below expression is derived:

$$\begin{aligned} &\overline{E}_1 e_1\beta_2^2\mu_2^2(e_2-\overline{e}_2)E_2 + E_2e_2\beta_1\mu_1\beta_2\mu_2(\overline{E}_1e_1 - E_2\overline{e}_2) + E_2\overline{e}_2\beta_1\mu_1\beta_2\mu_2(\overline{E}_1e_1 - E_2e_2) + \\ &\overline{E}_1\overline{e}_1\beta_2^2\mu_2^2(\overline{e}_2-e_2)E_2 + E_2e_2\beta_1\mu_1\beta_2\mu_2(\overline{E}_1\overline{e}_1 - E_2\overline{e}_2) + E_2\overline{e}_2\beta_1\mu_1\beta_2\mu_2(\overline{E}_1\overline{e}_1 - E_2e_2) + \\ &\overline{E}_1\overline{e}_1\beta_1\mu_1\beta_2\mu_2(E_2\overline{e}_2 - \overline{E}_1e_1) + \overline{E}_1e_1\beta_1\mu_1\beta_2\mu_2(E_2\overline{e}_2 - \overline{E}_1\overline{e}_1) + E_2\overline{e}_2\beta_1^2\mu_1^2(\overline{e}_1-e_1)\overline{E}_1 + \\ &\overline{E}_1\overline{e}_1\beta_1\mu_1\beta_2\mu_2(E_2e_2 - \overline{E}_1e_1) + \overline{E}_1e_1\beta_1\mu_1\beta_2\mu_2(E_2e_2 - \overline{E}_1\overline{e}_1) + E_2e_2\beta_1^2\mu_1^2(e_1-\overline{e}_1)\overline{E1} \\ &= 0 \end{aligned} \tag{A.3}$$

Using the property $e_1\overline{e}_1 = e_2\overline{e}_2 = \overline{e}_1 e_1 = \overline{e}_2 e_2 = 1$, equation A.3 becomes:

$$\begin{aligned}
&\overline{E}_1 e_1 \beta_2^2 \mu_2^2 (e_2 - \overline{e}_2) E_2 + E_2 \beta_1 \mu_1 \beta_2 \mu_2 (\overline{E}_1 e_1 e_2 - E_2) + E_2 \beta_1 \mu_1 \beta_2 \mu_2 (\overline{E}_1 e_1 \overline{e}_2 - E_2) + \\
&\overline{E}_1 \overline{e}_1 \beta_2^2 \mu_2^2 (\overline{e}_2 - e_2) E_2 + E_2 \beta_1 \mu_1 \beta_2 \mu_2 (\overline{E}_1 \overline{e}_1 e_2 - E_2) + E_2 \beta_1 \mu_1 \beta_2 \mu_2 (\overline{E}_1 \overline{e}_1 \overline{e}_2 - E_2) + \\
&\overline{E}_1 \beta_1 \mu_1 \beta_2 \mu_2 (E_2 \overline{e}_2 \overline{e}_1 - \overline{E}_1) + \overline{E}_1 \beta_1 \mu_1 \beta_2 \mu_2 (E_2 \overline{e}_2 e_1 - \overline{E}_1) + E_2 \overline{e}_2 \beta_1^2 \mu_1^2 (\overline{e}_1 - e_1) \overline{E}_1 + \\
&\overline{E}_1 \beta_1 \mu_1 \beta_2 \mu_2 (E_2 e_2 \overline{e}_1 - \overline{E}_1) + \overline{E}_1 \beta_1 \mu_1 \beta_2 \mu_2 (E_2 e_2 e_1 - \overline{E}_1) + E_2 e_2 \beta_1^2 \mu_1^2 (e_1 - \overline{e}_1) \overline{E1} \\
&= 0
\end{aligned} \tag{A.4}$$

factoring $(e_1 - \overline{e}_1)$ and $(e_2 - \overline{e}_2)$, equation A.4 becomes:

$$\begin{aligned}
&\overline{E}_1 \beta_2^2 \mu_2^2 (e_2 - \overline{e}_2)(e_1 - \overline{e}_1) E_2 + E_2 \beta_1^2 \mu_1^2 (e_1 - \overline{e}_1)(e_2 - \overline{e}_2) \overline{E}_1 + \\
&\overline{E}_1 E_2 \beta_1 \mu_1 \beta_2 \mu_2 (e_1 e_2 + e_2 \overline{e}_1 + e_1 \overline{e}_2 + \overline{e}_1 \overline{e}_2) - 4 E_2^2 \beta_1 \mu_1 \beta_2 \mu_2 \\
&\overline{E}_1 E_2 \beta_1 \mu_1 \beta_2 \mu_2 (e_1 e_2 + e_2 \overline{e}_1 + e_1 \overline{e}_2 + \overline{e}_1 \overline{e}_2) - 4 \overline{E}_1^2 \beta_1 \mu_1 \beta_2 \mu_2 \\
&= 0
\end{aligned} \tag{A.5}$$

factoring $(e_1 - \overline{e}_1)(e_2 - \overline{e}_2)$, equation A.5 becomes:

$$\begin{aligned}
&\overline{E}_1 E_2 (e_2 - \overline{e}_2)(e_1 - \overline{e}_1)(\beta_1^2 \mu_1^2 + \beta_2^2 \mu_2^2) + \\
&2 \overline{E}_1 E_2 \beta_1 \mu_1 \beta_2 \mu_2 (e_1 e_2 + e_2 \overline{e}_1 + e_1 \overline{e}_2 + \overline{e}_1 \overline{e}_2) \\
&- 4 \beta_1 \mu_1 \beta_2 \mu_2 (\overline{E}_1^2 + E_2^2) = 0
\end{aligned} \tag{A.6}$$

putting $\overline{E}_1$ and E_2 on one side of the equation

$$
\begin{aligned}
4\beta_1\mu_1\beta_2\mu_2\frac{(\overline{E}_1^2+E_2^2)}{\overline{E}_1E_2} =&(e_2-\overline{e}_2)(e_1-\overline{e}_1)(\beta_1^2\mu_1^2+\beta_2^2\mu_2^2)+ \\
&2\beta_1\mu_1\beta_2\mu_2(e_1+\overline{e}_1)(e_2+\overline{e}_2)
\end{aligned}
\tag{A.7}
$$

Since e_1, $\overline{e}_1$, e_2, and $\overline{e}_2$ obey the properties below:

$$
\begin{aligned}
(e_2-\overline{e}_2) =&2isin(\beta_2d_2) \\
(e_1-\overline{e}_1) =&2isin(\beta_1d_1) \\
(e_2+\overline{e}_2) =&2cos(\beta_2d_2) \\
(e_1+\overline{e}_1) =&2cos(\beta_1d_1) \\
\frac{(\overline{E}_1^2+E_2^2)}{\overline{E}_1E_2} =&\overline{E}_1\overline{E}_2+E_1E_2=2cos(k(d_1+d_2))
\end{aligned}
\tag{A.8}
$$

Using these equations A.8 into equation A.7, the desired S_h-dispersion relationship is found

$$
cos(k(d_1+d_2)) = cos(\beta_1)cos(\beta_2) - \frac{(m_1/m_2+m_2/m_1)}{2}sin(\beta_1)sin(\beta_2) \tag{A.9}
$$

with $m_j = \mu_j\beta_j$